ISSN 1063-7796, Physics of Particles and Nuclei, 2006, Vol. 37, No. 3, pp. 321–346. © Pleiades Publishing, Inc., 2006.

Some Aspects of Positronium Physics*

S. N. Gninenko[a], N. V. Krasnikov[a], V. A. Matveev[a], and A. Rubbia[b]

[a] *Institute for Nuclear Research, Russian Academy of Sciences, Moscow, 117312 Russia*
[b] *ETH Zürich, Zürich, Switzerland*
e-mail: gninenko@inr.ru, krasniko@ms2.inr.ac.ru, matveev@ms2.inr.ac.ru, Andre.Rubbia@cern.ch

Abstract—Some aspects of both theoretical and experimental study of the positronium system to probe physics beyond the Standard Model are reviewed. In particular, new experiments to search for the invisible decay of orthopositronium (o-Ps) with the sensitivity in the branching ratio Br(o-Ps $\longrightarrow$ invisible) $\simeq 10^{-8}$–10^{-7} are discussed. The experimental technique involves a specially designed high-efficiency pulsed slow positron beam, which is also applicable for other experiments with o-Ps in vacuum. Details of the beam design, as well as the first measurements results are presented. Possible applications of the slow-pulsed positron beam for materials research are discussed.

PACS number: 13.66.Hk

DOI: 10.1134/S1063779606030038

1. INTRODUCTION

Quantum electrodynamics (QED) is the textbook example of the success of quantum field theory. Many physical quantities (anomalous electron and muon magnetic moments; hyperfine splitting of hydrogen, muonium, and positronium; Lamb shift, etc.) have been calculated very precisely. The measurements have been characterized by excellent agreement with the theoretical predictions and in general have provided very clean conditions for hunting for small deviations from the standard theory.

Positronium (Ps), the positron–electron bound state, is the lightest known atom; it is bounded and self-annihilates through the same electromagnetic interaction. At the current level of experimental and theoretical precision, this is the only interaction present in this system. This feature has made positronium an ideal system for testing the accuracy of QED calculations for bound states, in particular, for the triplet (1^3S_1) state of Ps, orthopositronium (o-Ps). Due to the odd–parity under C-transformation, o-Ps decays predominantly into three photons. As compared with the singlet (1^1S_0) state (parapositronium), the "slowness" of the o-Ps decay rate due to the phase space and additional α suppression factors, gives an enhancement factor $\simeq 10^3$, making it more sensitive to an admixture of new interactions which are not accommodated in the Standard Model.

Positronium was discovered experimentally in 1951 by Deutsch [1], who observed its decay in different gases. Since then, a lot of focus has been set on the determination of its basic properties, including decay lifetime, decay modes, spectroscopy, etc. In particular, the measurement of the o-Ps lifetime attracted much attention.

Since 1989, the precision on the o-Ps lifetime reached a value well under 1000 ppm. Much excitement was aroused when the measurements performed by the Michigan group did not agree with theory. This problem, called the o-Ps lifetime puzzle, ignited much experimental and theoretical activity devoted to its clarification. This activity consisted in: (1) new direct lifetime measurements by the Tokyo group which did not confirm the discrepancy; (2) new theoretical calculations by Adkins et al. including higher-order terms improving the theoretical precision well below experimental errors, however, confirming early theoretical estimates; (3) searches for "exotic" decay modes which could explain the lifetime discrepancy at the cost of new physics (violation of basic conservation laws with decays into one photon, two photons; anomalous rate in five photons; millicharged particles; new bosons, etc.); (4) exotic suggestions for disappearance mechanisms (mirror worlds, extra dimensions). Recently, the Michigan group has published a new result, which is now in agreement with the theoretical value, somewhat in contradiction with the earlier results from the same group. At any rate, it should be noted that, as a light pure leptonic atom, positronium is a very specific probe for QED and new physics beyond the Standard Model.

The main goal of this paper is to review some aspects concerning both theoretical and experimental study of the positronium system to probe new physics beyond the Standard Model [2][1] (for theoretical and

* The text was submitted by the authors in English.

[1] It should be noted that there are several review articles that have surveyed tests of fundamental physics with positronium annihilation [3–12].

experimental reviews of the precision tests of the bound-state QED, see, e.g., [3], and the recent work [4]).

The paper is organized as follows. In Section 2, we review the status of QED calculations for positronium and experimental results on standard positronium decays. In Section 3, we review the experimental bounds for exotic positronium decays and discuss the search for discrete symmetries violation in positronium decays. In Section 4, some models (mirror matter, additional dimensions, etc.), which predict interesting (from the experimental point of view) rare positronium decays are presented. In Section 5, we describe new experiments dedicated to the search for orthopositronium invisible decay mode. The new high-efficiency pulse positron beam, the description of the pulsing system design, and the first measurement results obtained with the beam are presented in Section 6. Possible applications of the developed pulsed beam for measurements in materials research are discussed in Section 7. A summary is given in Section 8.

2. STATUS OF QED CALCULATIONS

The present theoretical knowledge of the decay rates (widths) of the $^3S_1$ orthopositronium (o-Ps) and $^1S_0$ parapositronium (p-Ps) ground states to three and two photons, respectively, may be summarized as follows [13]:

$$\Gamma_o^{\rm th} = \frac{2(\pi^2-9)\alpha^6 m_e}{9\pi}\left\{1-\frac{\alpha}{\pi}10.286606(10)\right.$$
$$+\left(\frac{\alpha}{\pi}\right)^2\left[\frac{\pi^2}{3}\ln\alpha+44.87(26)\right]+\frac{\alpha^3}{\pi}\left[-\frac{3}{2}\ln^2\alpha\right. \quad (1)$$
$$\left.\left.+\left(3.428869(3)-\frac{229}{30}-8\ln 2\right)\ln\alpha+\frac{D_o}{\pi^2}\right]\right\},$$

$$\Gamma_p^{\rm th} = \frac{\alpha^5 m_e}{2}\left\{1+\frac{\alpha}{\pi}\left(\frac{\pi^2}{4}-5\right)\right.$$
$$+\left(\frac{\alpha}{\pi}\right)^2[-2\pi^2\ln\alpha+5.1243(33)]+\frac{\alpha^3}{\pi}\left[-\frac{3}{2}\ln^2\alpha\right. \quad (2)$$
$$\left.\left.+\left(\frac{533}{90}-\frac{\pi^2}{2}+10\ln 2\right)\ln\alpha+\frac{D_p}{\pi^2}\right]\right\}.$$

The first-order corrections to o-Ps and p-Ps decay rates were found in [14, 15]. The logarithmically enhanced second-order corrections were obtained in [16, 17]. Recently, the calculation of the nonlogarithmic second-order corrections has been completed in [18, 19]. In the third order, only the double logarithmic [20] and single logarithmic corrections [21] are known.[2] The coefficients $D_{o,p}$ parametrize the unknown nonlogarithmic $O(\alpha^3)$ terms. The o-Ps decays into five photons and p-Ps decays into four photons, which are not included in Eqs. (1) and (2), lead to an increase in the numerical coefficients in front of $(\alpha/\pi)^2$ by 0.187(11) and 0.274290(8), respectively [22]. Including all the terms known so far, we obtain for the p-Ps and o-Ps total decay rates

$$\Gamma_o^{\rm th} = 7.039979(11)\ \mu{\rm s}^{-1}, \quad (3)$$

$$\Gamma_p^{\rm th} = 7989.6178(2)\ \mu{\rm s}^{-1}, \quad (4)$$

where the given errors stem only from the uncertainty in the numerical values of the perturbative coefficients.

Note that experimental study of the o-Ps decay rate has a colorful history of inconsistent results and poor agreement with theoretical predictions (see [23] for a review). The most recent independent measurements in SiO_2 powder [24] and vacuum [25] experiments

$$\Gamma_o^{\rm exp} = 7.0396(12)^{\rm stat.}(11)^{\rm syst.}\ \mu{\rm s}^{-1}\ (SiO_2\ \text{powder}), \quad (5)$$

$$\Gamma_o^{\rm exp} = 7.0404(10)^{\rm stat.}(8)^{\rm syst.}\ \mu{\rm s}^{-1}\ (\text{vacuum}), \quad (6)$$

however, are consistent with each other and are in a very good agreement with Eq. (3). The Michigan group attribute the major systematic effect to the *intensity* of the backscattered o-Ps component, which depends on the incident positrons energy and the target material [25]. Taking into account the collisional annihilation of these o-Ps's on the vacuum cavity walls results in a big (~350 ppm) correction to $\Gamma_o^{\rm exp}$ obtained in their previous measurements [30]. In their last measurements, the effect was minimized by using a special thin nanoporous silica target and taken into account [25] (for more discussions, see, e.g., [27]).

The most recent experimental data on p-Ps decay rate [26]

$$\Gamma_p^{\rm exp} = 7990.9(1.7)\ \mu{\rm s}^{-1} \quad (7)$$

is also consistent with Eq. (4) within the error bars.[3] The measurements of the o-Ps lifetime performed after 1987 are summarized in Table 1 and Fig. 1.

Positronium hyperfine splitting (HFS), $\Delta\nu = E(1^3S_1) - E(1^1S_0)$, where $E(1^1S_0)$ and $E(1^3S_1)$ are the energy levels of p-Ps and o-Ps ground state, is the most precisely measured quantity in positronium spectroscopy as far

[2] In Eq. (1), the nonanalytic part of the $\alpha^3\ln\alpha$ coefficient represents the interference between the first-order correction and the second-order logarithmic term.

[3] Note that the singlet decay rate has been measured using magnetic singlet–triplet state mixing in a gas mixture. Therefore, the accuracy of $\Gamma_p^{\rm exp}$ is affected by the precision of $\Gamma_o^{\rm exp}$ measurements in the experiment of [30].

Table 1. Experimental and theoretical results on the *o*-Ps decay rate

Year	Group, reference	Rate, μs^{-1}	Errors, ppm	Technique	Exp – th	Exp – th (sigma)
1987	Ann Arbor [28]	7.0516	180	Gas	0.01162	8.9
1989	Ann Arbor [29]	7.0514	200	Gas	0.01142	8.2
1990	Ann Arbor [30]	7.0482	230	Vacuum	0.00822	5.1
1995	Tokyo [24]	7.0398	412	Powder	–0.00018	–0.06
2000	Tokyo [31]	7.0399	412	Powder	–0.00008	0.0
2003	Ann Arbor [25]	7.0404	185	Vacuum	0.00042	0.32
2003	Tokyo [32]	7.0396	227	Powder	–0.00038	0.024
2000	AFS [18]	7.039979	1.6	Theory		

as absolute precision is concerned. The most recent measurements of HFS yielded [33, 34]

$$\Delta\nu^{\rm exp} = 203.3875(16)\ \text{GHz}, \tag{8}$$

$$\Delta\nu^{\rm exp} = 203.38910(74)\ \text{GHz}. \tag{9}$$

On the theoretical side, we have

$$\begin{aligned}\Delta\nu^{\rm th} &= \frac{7m_e\alpha^4}{12}\left\{1-\frac{\alpha}{\pi}\left(\frac{32}{21}+\frac{6}{7}\ln 2\right)\right.\\ &+\left(\frac{\alpha}{\pi}\right)^2\left[-\frac{5}{14}\pi^2\ln\alpha+\frac{1367}{378}-\frac{5197}{2016}\pi^2\right.\\ &\left.+\left(\frac{6}{7}+\frac{221}{84}\pi^2\right)\ln 2-\frac{159}{56}\zeta(3)\right]\\ &\left.+\frac{\alpha^3}{\pi}\left[-\frac{3}{2}\ln^2\alpha-\left(\frac{62}{15}-\frac{68}{7}\ln 2\right)\ln\alpha+\frac{D_\nu}{\pi^2}\right]\right\}.\end{aligned} \tag{10}$$

The first-order correction was calculated in [35]. The logarithmically enhanced second-order correction was found in [16, 36]. The nonlogarithmic second-order term includes the contribution due to the radiative correction to the Breit potential [37], the three-, two-, and one-photon annihilation contributions [38], the nonannihilation radiative recoil contribution [39], and the pure recoil correction computed numerically in [40] and analytically in [41]. In the third order, as in the case of the decay rates, only the double logarithmic [20] and single logarithmic corrections [42] are known. Collecting all the available contributions, we get

$$\Delta\nu^{\rm th} = 203.39169\ \text{GHz}, \tag{11}$$

which exceeds Eqs. (8) and (9) by approximately 2.6 and 3.5 experimental standard deviations, respectively. As far as pure QED predictions are concerned, the accuracy of the current theoretical estimates is determined by the missing nonlogarithmic $O(\alpha^3)$ terms. To estimate the corresponding uncertainty, we may speculate about the magnitudes of the coefficients $D_{o,p,\nu}$. Substituting the numerical values for the perturbative coefficients in Eqs. (1), (2), and (10), we get

$$\begin{aligned}\Gamma_o^{\rm th} &= \Gamma_o^{\rm LO}\left(1-3.27\alpha+0.33\alpha^2\ln\alpha\right.\\ &\left.+4.53\alpha^2-0.48\alpha^3\ln^2\alpha-1.76\alpha^3\ln\alpha+\frac{D_o}{\pi^3}\alpha^3\right),\end{aligned} \tag{12}$$

$$\begin{aligned}\Gamma_p^{\rm th} &= \Gamma_p^{\rm LO}\left(1-0.81\alpha-2.00\alpha^2\ln\alpha\right.\\ &\left.+0.55\alpha^2-0.48\alpha^3\ln^2\alpha+2.52\alpha^3\ln\alpha+\frac{D_p}{\pi^3}\alpha^3\right),\end{aligned} \tag{13}$$

$$\begin{aligned}\Delta\nu &= \Delta\nu^{\rm LO}\left(1-0.67\alpha-0.36\alpha^2\ln\alpha\right.\\ &\left.-0.67\alpha^2-0.48\alpha^3\ln^2\alpha+0.83\alpha^3\ln\alpha+\frac{D_\nu}{\pi^3}\alpha^3\right).\end{aligned} \tag{14}$$

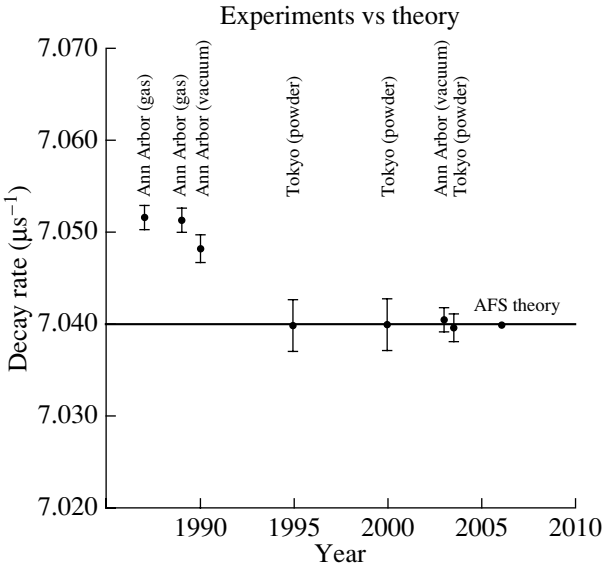

Fig. 1. Summary of the experimental results on *o*-Ps lifetime measurements as a function of the year. The last point is the theoretical value from AFS [18].

Table 2. Theoretical vs. experimental errors (see text)

	Theory	Experiment
$\Delta\Gamma_o$	$1.4 \times 10^{-5}\ \mu s^{-1}$	$1.3 \times 10^{-3}\ \mu s^{-1}$
$\Delta\Gamma_p$	$1.6 \times 10^{-2}\ \mu s^{-1}$	$1.7\ \mu s^{-1}$
$\Delta\nu$	400 kHz	740 kHz

The perturbative coefficients do not systematically increase in magnitude with the order of the expansion if α (not α/π) is taken as the formal expansion parameter. Thus, one can estimate [13] the numerical value of $D_{o,p,\nu}/\pi^3$ to be a few units, which is a typical number in Eqs. (12)–(14). This naive extrapolation is supported by the explicit result for the radiative corrections to HFS in muonium, where the corresponding coefficient reads [43, 44]

$$\frac{D_\nu^{(\mu^+e^-)}}{\pi^3} \approx 5. \tag{15}$$

If the coefficients $D_{o,p,\nu}$ do not have absolute magnitudes in excess of Eq. (15), then the uncertainties due the lack of their knowledge fall within the errors quoted in Table 2 [13]. For comparison, the minimal reported experimental errors are also included in this table.[4]

Further progress in the investigation of positronium decays now crucially depends on the reduction of the experimental errors, which now greatly exceed the theoretical one. The experimental error for HFS is compatible with a naive estimate of the theoretical uncertainty due to as yet unknown higher-order corrections. Should this discrepancy persist after the dominant terms of the latter have been calculated and the experimental accuracy has been increased, this would provide a signal for new physics. This makes the HFS one of the most interesting topics in positronium spectroscopy both from the experimental and theoretical points of view.

The annihilation of p-Ps to four photons to the lowest order is [45] $\Gamma_{LO}(4\gamma) = 0.013893 m\alpha^7$. The one-loop correction to the four-photon decay rate was calculated to be [46]

$$\Gamma(4\gamma) = \Gamma_{LO}(4\gamma)\left[1 - \frac{\alpha}{\pi} + O(\alpha^2)\right], \tag{16}$$

yielding $\mathrm{Br}(o\text{-Ps} \longrightarrow 4\gamma) = 1.4388 \times 10^{-6}$. Experimental data are in agreement with theoretical calculations (see [12]). The five-photon o-Ps $\longrightarrow 5\gamma$ decay branching ratio is of order α^2 [47]

$$\mathrm{Br}(o\text{-Ps} \longrightarrow 5\gamma) = 0.19(1)\left(\frac{\alpha}{\pi}\right)^2 \approx 1.0 \times 10^{-6} \tag{17}$$

[4] If given separately, the statistic and systematic errors are added up in quadrature.

and, therefore, does not significantly influence the total decay width. Experimental result on o-Ps $\longrightarrow 5\gamma$ decay gives [48]

$$\mathrm{Br}(o\text{-Ps} \longrightarrow 5\gamma) = [2.2^{+2.6}_{-1.6}(\mathrm{stat.}) \pm 0.5(\mathrm{syst.})] \times 10^{-6} \tag{18}$$

in agreement with the theoretical prediction of Eq. (17).

Within the Standard Model, orthopositronium can also decay weakly into a neutrino–antineutrino pair. The o-Ps $\longrightarrow \nu_e\bar{\nu}_e$ decay occurs through W exchange in t channel and e^+e^- annihilation via Z. The decay width is [49]

$$\Gamma(o\text{-Ps} \longrightarrow \nu_e\bar{\nu}_e) = \frac{G_F^2\alpha^3 m_e^2}{24\pi^2}(1 + 4\sin^2\theta_W)^2 \approx 6.2 \times 10^{-18}\Gamma_o^{\mathrm{exp}}. \tag{19}$$

For other neutrino flavors, only Z-diagram contributes. For $l \neq e$, the decay width is [49]

$$\Gamma(o\text{-Ps} \longrightarrow \nu_l\bar{\nu}_l) = \frac{G_F^2\alpha^3 m_e^2}{24\pi^2}(1 - 4\sin^2\theta_W)^2 \approx 9.5 \times 10^{-21}\Gamma_o^{\mathrm{exp}}. \tag{20}$$

Thus, in the Standard Model, the o-Ps $\longrightarrow \nu\bar{\nu}$ decay width is too small and its contribution to the total decay width can also be neglected.

3. EXPERIMENTAL BOUNDS ON EXOTIC ORTHOPOSITRONIUM DECAYS

Visible exotic decays of o-Ps can be classified into the three following categories: (i) o-Ps $\longrightarrow \gamma X$, (ii) o-Ps $\longrightarrow \gamma\gamma X$, and (iii) o-Ps $\longrightarrow N\gamma$, where X is a new light particle(s) and $N = 2, 4, \ldots$ (for review, see, e.g., [5, 11, 12]).

The decay o-Ps $\longrightarrow 4\gamma$ is forbidden by C-invariance. The corresponding experimental bound is [51]

$$\mathrm{Br}(o\text{-Ps} \longrightarrow 4\gamma) < 2.6 \times 10^{-6}. \tag{21}$$

The o-Ps has spin one, so it cannot decay into two photons due to conservation of angular momentum. Since angular momentum conservation follows from the isotropy of space, searching for decays o-Ps $\longrightarrow 2\gamma$ tests spatial isotropy. The best current result is [53]

$$\mathrm{Br}(o\text{-Ps} \longrightarrow 2\gamma) < 3.5 \times 10^{-6}. \tag{22}$$

For the decay o-Ps $\longrightarrow \gamma + X$, where X is a long-lived particle, the experimental bound is [54]

$$\mathrm{Br}(o\text{-Ps} \longrightarrow \gamma + X) < 1.1 \times 10^{-6},\ (m_X < 800\ \mathrm{keV}). \tag{23}$$

If X decays within detector, e.g., into 2γ, the experimental bounds depend on the X-particle mass [56–59]:

$$\mathrm{Br}(o\text{-Ps} \longrightarrow \gamma + X \longrightarrow 3\gamma) < 2 \times 10^{-4},\ (300\ \mathrm{KeV} < m_X < 900\ \mathrm{keV}), \tag{24}$$

$$\mathrm{Br}(o\text{-Ps} \longrightarrow \gamma + X \longrightarrow 3\gamma) < 2.8 \times 10^{-5}, \quad (m_X < 30\ \mathrm{keV}), \tag{25}$$

$$\mathrm{Br}(o\text{-Ps} \longrightarrow \gamma + X \longrightarrow 3\gamma) < 2 \times 10^{-5}, \quad (900 < m_X < 1013\ \mathrm{keV}). \tag{26}$$

The negative search for direct e^+e^- annihilation $e^+e^- \longrightarrow \gamma + X$ leads for the case of long-lived X particle to the bounds [60]:

$$\mathrm{Br}(o\text{-Ps} \longrightarrow 2\gamma + X) < 4.2 \times 10^{-6}, \quad (m_X < 200\ \mathrm{keV}), \tag{27}$$

$$\mathrm{Br}(o\text{-Ps} \longrightarrow 2\gamma + X) < 2.1 \times 10^{-5}, \quad (m_X < 2m_e). \tag{28}$$

In [61], more stringent bound

$$\mathrm{Br}(o\text{-Ps} \longrightarrow 2\gamma + X) < 4 \times 10^{-6} \tag{29}$$

has been obtained.

Note that all the above limits are based on a search for a peak in the energy spectrum of photons arising from the two-body decay of o-Ps. In the case of possible exotic three-body o-Ps $\longrightarrow \gamma + X_1 + X_2$ decay, which still might be a solution of the o-Ps decay puzzle [11, 62], the signal cannot manifest itself through the peak in the γ energy spectrum, thus making the experimental search for this decay mode more difficult. The existing estimate of the corresponding bound on $\mathrm{Br}(o\text{-Ps} \longrightarrow \gamma X_1 X_2)$ from the results of the indirect experiment of [63] is around 10^{-4} [11]. Recent ETHZ–Moscow experiment [64] on the search for exotic decay o-Ps $\longrightarrow \gamma + X_1 + X_2$ leads to the bound $\mathrm{Br}(o\text{-Ps} \longrightarrow \gamma X_1 X_2) \le 4.4 \times 10^{-5}$ for $m_{X_1} + m_{X_2} < 900$ keV.

The experimental signature of the o-Ps $\longrightarrow$ *invisible* decay is the absence of an energy deposition of ~1 MeV, which is expected from the ordinary o-Ps annihilation, in a 4π calorimeter surrounding the o-Ps formation region. The first experiment on o-Ps $\longrightarrow$ *invisible* decay was performed a long time ago [65] and then was repeated with a higher sensitivity by Mitsui et al. [63]. The best current experimental bound is [63]

$$\mathrm{Br}(o\text{-Ps} \longrightarrow \textit{invisible}) < 2.8 \times 10^{-6}. \tag{30}$$

Let us now discuss the implications of the C, P, T, CP, CPT symmetries for positronium decays (see, e.g., [67, 68]). For the positronium system with orbital momentum l and total spin S, C-parity is $C = (-1)^{l+S}$ and P-parity is $P = (-1)^{l+1}$. In particular, for parapositronium and orthopositronium, we have $J^{PC}_{p\text{-Ps}} = 0^{-+}$, $J^{PC}_{o\text{-Ps}} = 1^{--}$. Other positronium states have quantum numbers $n^{2S+1}L_{JPC} = 2^1S_{0^{-+}}$, $2^3P_{0^{++}}$, $2^3P_{1^{++}}$, $2^3P_{1^{+-}}$, $2^3P_{2^{++}}$, $2^3S_1^{--}$, ….

As a consequence of C-invariance, the following decays are prohibited:

$$p\text{-Ps} \longrightarrow 3\gamma, 5\gamma\ldots, \tag{31}$$

$$o\text{-Ps} \longrightarrow 4\gamma, 6\gamma\ldots. \tag{32}$$

The corresponding experimental limits are [51]

$$\mathrm{Br}(o\text{-Ps} \longrightarrow 4\gamma) < 2.6 \times 10^{-6}, \tag{33}$$

$$\mathrm{Br}(p\text{-Ps} \longrightarrow 3\gamma) < 2.8 \times 10^{-6}. \tag{34}$$

Other interesting one-photon decays, which are prohibited by C-invariance, are

$$2^3S_{1^{--}} \longrightarrow 1^3S_{1^{--}} + \gamma, \tag{35}$$

$$2^1P_{1^{+-}} \longrightarrow 1^3S_{1^{--}} + \gamma. \tag{36}$$

Note that the system of two photons with $J = 0$ can be in two states

$$|+\rangle \equiv \frac{1}{\sqrt{2}}(|{+}{+}\rangle + |{-}{-}\rangle), \quad (\eta_P = +1), \tag{37}$$

$$|-\rangle \equiv \frac{1}{\sqrt{2}}(|{+}{+}\rangle - |{-}{-}\rangle), \quad (\eta_P = -1). \tag{38}$$

Parapositronium p-Ps decays into the $|-\rangle$ state.

As mentioned in [106], in p-Ps decays, a nonzero asymmetry in the helicity for the decay width

$$\delta\Gamma \sim \frac{(\vec{k}_1\vec{s}_1)}{|\vec{k}_1|} = \lambda_1 \tag{39}$$

violates the CPT-symmetry. Here, $\vec{k}_1$ and $\vec{s}_1$ are the momentum and spin of one of the two photons. Note that the interaction in the final state can imitate CPT-violation. For the case of p-Ps to two-photon decay, the mixing of p-Ps($J^{PC} = 0^{-+}$) with $2^3P_0^{++}$ can also imitate CPT-violation. For o-Ps decays, the Bernreuther–Nachtmann correlation [69] $\delta\Gamma(o\text{-Ps} \longrightarrow 3\gamma) \sim \vec{s} \cdot \vec{k}_1 \times \vec{k}_2$ violates the CPT-symmetry. This correlation is T-odd and P-even. The experiment [70] restricts this correlation to the level of 2.3%. Another interesting correlation for the o-Ps $\longrightarrow 3\gamma$ decay width is

$$\delta\Gamma \sim \vec{s} \cdot \vec{k}_1. \tag{40}$$

This correlation violates both P- and CPT-symmetries. The correlation

$$\delta\Gamma \sim (\vec{s} \cdot \vec{k}_1)(\vec{s} \cdot \vec{k}_1 \times \vec{k}_2) \tag{41}$$

violates both P- and T-symmetries and conserves the CPT-symmetry. Here, $\vec{s}$ is the positronium spin and $\vec{k}_1$, $\vec{k}_2$ are the momenta of the two photons with highest

Table 3. Upper limits on the branching ratios of several exotic *o*-Ps decays

Decay mode	90% upper limit, ppm	Comments	Group
		Long-lived *X*-boson	
$\gamma + X$	5–1	$m_X \sim 100$–900 keV	CERN [50]
	1.1	$m_X < 800$ keV	Tokyo [54]
	340	$m_X < 30$ keV	Moscow [59]
		Short-lived *X*-boson	
$\gamma + X \longrightarrow \gamma + 2\gamma$	28	$m_X < 30$ keV	Moscow [57]
	300	$m_X < 500$ keV	Tokyo [55]
$\gamma\gamma$	233	Forbidden by angular momentum conservation	Michigan [52]
	350		Tokyo [53]
$\gamma\gamma\gamma$	2.6	Forbidden by *C*-parity	Tokyo [51], Berkeley [66]
	3.7		
$\gamma + X_1 + X_2$	44	$m_{X_1} + m_{X_2} < 900$ keV	ETHZ-Moscow [64]
Invisible	2.8	Not in vacuum	Tokyo [63]
	540		Moscow [65]

energies. This correlation is compatible with zero at 1% level of accuracy [71]. A new experiment has been proposed [72], which will be able to increase the accuracy by two orders of magnitude.

It is important to stress that there are two ways to test discrete symmetries in positronium decays. Namely, we can look for prohibited decays like:

$$p\text{-Ps} \longrightarrow 3\gamma \text{ (}C\text{-invariance)},$$
$$o\text{-Ps} \longrightarrow 4\gamma \text{ (}C\text{-invariance)},$$
$$o\text{-Ps} \longrightarrow 2\gamma \text{ (isotropy of space)},$$

or we can look for *C*, *P*, …, *CPT*-violating correlations in positronium decays like:

$$p\text{-Ps} \longrightarrow 2\gamma; \quad \delta\Gamma \sim \frac{(\vec{k}_1 \vec{s}_1)}{|\vec{k}_1|},$$

$$o\text{-Ps} \longrightarrow 3\gamma; \quad \delta\Gamma \sim \vec{s} \cdot \vec{k}_1 \times \vec{k}_2.$$

In Table 3, bounds on exotic orthopositronium decay modes are summarized. Discussion of possible future experiments on the search for discrete symmetries violations in positronium decays can be found in [72].

4. ORTHOPOSITRONIUM EXOTIC DECAY MODELS

Consider several motivations for further experimental searching for positronium exotic decay modes.

4.1. Millicharged Particles

In 1986, Holdom [73] showed that, by adding a second, unobserved, photon (the "shadow" photon), one could construct Grand Unified Models which contain particles with an electric charge very small compared to the natural electron charge. This work has stimulated new theoretical and experimental tests (for a recent review, see [74] and references therein). If such *millicharged particles* with low mass exist, the *o*-Ps would decay into it invisibly, since the particles would penetrate any type of calorimeter mostly without interaction. The corresponding decay width is [75]

$$\Gamma(o\text{-Ps} \longrightarrow X\bar{X}) = \frac{\alpha^5 Q_X^2 m_e}{6} k F\left(\frac{m_X^2}{m_e^2}\right), \qquad (42)$$

where Q_X is an electric charge of the *X*-particle ($Q_e \equiv 1$), $k = 1$, $F(x) = \left(1 - \frac{1}{2}x\right)(1-x)^{\frac{1}{2}}$ for spin $\frac{1}{2}$ and $k = \frac{1}{4}$, $F(x) = (1-x)^{\frac{3}{2}}$ for spinless *X*-particle. For spin-$\frac{1}{2}$ millicharged *X*-particle and for $m_X \ll m_e$, one can find from experimental bound (30) that $Q_X \le 8.6 \times 10^{-5}$ [63]. A search for millicharged particles through the *o*-Ps $\longrightarrow$ *invisible* decay with the sensitivity to Br(*o*-Ps $\longrightarrow$ *invisible*) $\approx 10^{-8}$ would intersect the parameter space, which is not excluded by results of the recent direct experiment at SLAC [76].

4.2. Mirror World

In 1956, Lee and Yang proposed [77] that the weak interactions of fundamental particles were not invariant under the parity transformation. The offered this suggestion to explain some experimental results that were considered as puzzles. They pointed out that these puzzles could be explained if one assumed a left–right

asymmetry in the weak interactions. In their original paper, they also provided a "remedy" for this a priori not sensible assumption. Indeed, Lee and Yang argued [77] that if left–right asymmetry were found in weak interactions, the question could still be raised whether there might exist corresponding elementary particles exhibiting opposite asymmetry such that, in the broader sense, there will still be overall right–left symmetry. They spoke specifically of two kinds of protons, the left-handed and the right-handed one. As is well-known, the left-handed nature of ordinary matter was brilliantly confirmed experimentally. Nowadays, parity violation in fundamental interactions is so well-accepted that the left–right asymmetry of Nature is inserted in the modern Standard Model "from the beginning" in the assignment of the particle fields. Nonetheless, the question of whether or not Nature is fundamentally left–right symmetric has remained up to now unresolved.

Landau was always convinced by the absolute symmetry of vacuum [78]. Under his appeal, Kobzarev, Okun, and Pomeranchuk suggested the hypothesis of a "mirror world" and discussed its phenomenological implications [79]. Today's mirror matter models exist in two basic versions. The symmetric version proposed earlier was further developed and put into a modern context by Foot, Lew, and Volkas [80]. The asymmetric version was proposed by Berezhiani and Mohapatra [81]. More detailed discussions of mirror matter models can be found in [82, 83].

It is fair to say that the existence of mirror matter has recently begun to attract more support since the realization of its possible connection to the dark matter problem [84]. If the total energy density of the Universe is composed of baryonic matter (~5%), nonbaryonic (invisible) dark matter (~25%), and dark energy (~70%), as recent astrophysical observations seem to indicate, then this clearly motivates the search for new kinds of matter, since the current Standard Model does not contain any heavy, stable nonbaryonic particles.[5] The basic concept is to have a theory given by the product $G \times G'$ of two identical gauge factors with the identical particle contents, which could naturally emerge, e.g., in the context of $E_8 \times E_8'$ superstring.

As discussed by Foot [86], the ordinary and mirror particles could form parallel sectors each with gauge symmetry G (where $G = G_{SM} \equiv SU(3)_c \otimes SU(2)_L \otimes U(1)_Y$ in the simplest case), so that the full gauge group is $G \otimes G$. Mathematically, mirror symmetry has the form [80]

$$\begin{gathered} x \longrightarrow -x, \quad t \longrightarrow t, \\ W^\mu \longleftrightarrow W'_\mu, \quad B^\mu \longleftrightarrow B'_\mu, \quad G^\mu \longleftrightarrow G'_\mu, \\ l_{iL} \longleftrightarrow \gamma_0 l'_{iR}, \quad e_{iR} \longleftrightarrow \gamma_0 e'_{iL}, \quad q_{iL} \longleftrightarrow \gamma_0 q'_{iR}, \\ u_{iR} \longleftrightarrow \gamma_0 u'_{iL}, \quad d_{iR} \longleftrightarrow \gamma_0 d'_{iL}, \end{gathered} \tag{43}$$

where G^μ, W^μ, and B^μ are the standard G_{SM} gauge particles; l_{iL}, e_{iR}, q_{iL}, u_{iR}, and d_{iR} are the standard leptons and quarks ($i = 1, 2, 3$ is the generation index); and the primes denote the mirror particles.

Ordinary and mirror particles couple with each other via gravity and possibly by new interactions connecting ordinary and mirror particles together. Constraints from gauge invariance, mirror symmetry and renormalizability, suggest only two types of new interactions [86]: (a) Higgs–mirror Higgs quartic coupling ($L = \lambda' \phi'^\dagger \phi' \phi^\dagger \phi$) and (b) via photon–mirror photon kinetic mixing:

$$L_{\text{int}} = \frac{\epsilon}{2} F^{\mu\nu} F'_{\mu\nu}, \tag{44}$$

where $F^{\mu\nu}$ ($F'_{\mu\nu}$) is the field strength tensor for electromagnetism (mirror electromagnetism). The effect of photon–mirror photon kinetic mixing is to cause mirror charged particles to couple to ordinary photons with effective electric charge ϵe [73, 80, 88].

Glashow pointed out [89] that a sensitive laboratory test for mirror matter could come from the orthopositronium system. Indeed, if the interaction of Eq. (44) exists, orthopositronium is connected via a one-photon annihilation diagram to its mirror version (o-Ps') (see Fig. 2). This breaks the degeneracy between o-Ps and o-Ps', so that the vacuum energy eigenstates are (o-Ps + o-Ps')/$\sqrt{2}$ and (o-Ps – o-Ps')/$\sqrt{2}$, which are split in energy by $\Delta E = 2h\epsilon f$, where $f = 8.7 \times 10^4$ MHz is the contribution to the ortho–para splitting from the one-photon annihilation diagram involving o-Ps [89]. Thus, the interaction eigenstates are maximal combinations of mass eigenstates, which implies that o-Ps oscillates into o-Ps' with probability

$$P(o\text{-Ps} \longrightarrow o\text{-Ps}') = \sin^2 \omega t, \tag{45}$$

where $\omega = \Delta E$.

In an experiment, mirror orthopositronium decays are not detected, hence leading to o-Ps $\longrightarrow$ *invisible* decays, which means that the number of orthopositronium, N, satisfies [89]

$$N = \cos^2 \omega t e^{-\Gamma^{3\gamma} t} \approx \exp[-t(\Gamma^{3\gamma} + \omega^2 t)], \tag{46}$$

where $\Gamma^{3\gamma}$ is the standard orthopositronium decay rate. Evidently, the observational effect of the oscillations is to the apparent decay rate of ordinary orthopositronium: $\Gamma^{\text{eff}} \approx \Gamma^{3\gamma}(1 + \omega^2/\Gamma^{3\gamma})$. This implies that the existence of mirror matter can be probed with positronium either (1) via a precision measurement of its decay rate and/or shape of its decay time spectrum or (2) via a direct search for invisible decays.

In the simplest case of o-Ps $\longrightarrow$ o-Ps' oscillations in vacuum [89], the branching ratio Br(o-Ps $\longrightarrow$ *invisi-*

[5] For more recent interesting ideas on searching for mirror matter, see [85] and references therein.

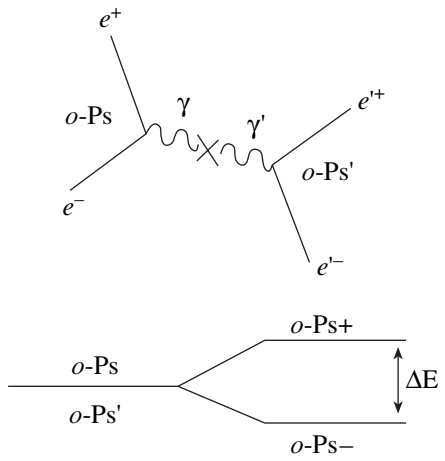

Fig. 2. The double degeneracy between orthopositronium mass eigenstates of ordinary *o*-Ps and mirror *o*-Ps' is broken when a small mixing (upper picture) term is included.

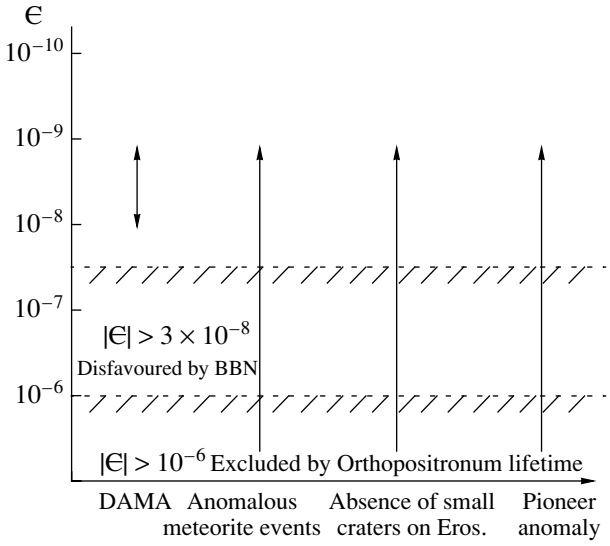

Fig. 3. Summary of the experimental constraints for ϵ by Foot [91].

ble) = $\Gamma_{inv}/\Gamma_{3\gamma}$ occurring during a long enough observation time can be calculated as

$$\mathrm{Br}(o\text{-Ps} \longrightarrow \textit{invisible}) = \frac{2(2\pi\epsilon f)^2}{\Gamma_{3\gamma}^2 + 4(2\pi\epsilon f)^2}. \quad (47)$$

However, Eq. (47) may not be applicable to all measurements. In experiments, orthopositronium is not produced in vacuum, but rather by slow positron collisions with a positronium formation target. As a result, the newly formed positronium will undergo elastic collisions with the target at a rate, Γ_{coll}, which depends on the particular experiment. These collisions cause quantum decoherence, disrupting the ordinary–mirror oscillations [90]. For the case where the collision rate is much larger than the decay rate, $\Gamma_{coll} \gg \Gamma_{3\gamma}$, the observed decay rate is approximately given by [87]

$$\Gamma_{obs} \simeq \Gamma_{3\gamma} + \frac{2\omega^2}{\Gamma_{coll}} = \Gamma_{3\gamma}\left(1 + \frac{2(2\pi\epsilon f)^2}{\Gamma_{coll}\Gamma_{3\gamma}}\right). \quad (48)$$

Thus, compared to Eq. (47), the branching ratio is suppressed roughly by a factor $\simeq\Gamma_{3\gamma}/\Gamma_{coll}$. In addition, external fields might result in a loss of coherence due to additional splitting of mass eigenstates [90].

Foot [91] discussed the possible importance of mirror matter in the context of the dark matter puzzle: if mirror matter is identified with the dark matter in the Universe, then it is natural to interpret the dark matter halo of our Galaxy as containing mirror matter (possibly, mirror stars/planets/dust and gas [91]). If the dark matter halo of our Galaxy is composed of mirror matter, then it can potentially be detected in dark matter experiments via the nuclear recoil signature via interactions between nuclei and mirror nuclei induced by the photon–mirror photon kinetic term mixing.

Very strikingly, Foot pointed out [91] that the DAMA results [92] could be interpreted in terms of such interaction, if one interprets the signal in terms of mirror O', Fe' mixture with an annual modulation effect in the 2–6 keV window:

$$|\epsilon|\sqrt{\frac{\xi_{O'}}{0.10} + \frac{\xi_{Fe'}}{0.02}} \simeq 4.5 \times 10^{-9}, \quad (49)$$

where $\xi_{A'} \equiv \rho_{A'}/(0.3\ \mathrm{GeV/cm^3})$ is the A' proportion (by mass) of the halo dark matter.[6] This is an extremely impressive result, which provides an indication for possible values of ϵ. These are summarized in Fig. 3 by Foot [91]. An interesting region, which seems also to be in the range of naturally small ϵ motivated by Grand Unification models as discussed by Berezhiani [82], is

$$10^{-9} \le \epsilon \le 10^{-8}. \quad (50)$$

Using Eq. (45), this implies

$$10^{-8} < \mathrm{Br}(o\text{-Ps} \longrightarrow \textit{invisible}) < 10^{-6}. \quad (51)$$

Interestingly, the values of ϵ from Eq. (50) are also consistent with all other known experimental and cosmological bounds including SN1987a[7] and the standard Big Bang nucleosynthesis (BBN) bound deduced from the successful prediction of the primordial ^{4}He abundance [93]:

$$\epsilon < 3 \times 10^{-8} \quad (52)$$

and, respectively,

[6] The DAMA Project at the Gran Sasso Laboratory (Italy) is an observatory for rare processes. One of the main activities is the investigation on dark matter particles in the galactic halo.

[7] The SN1987a limit $\epsilon < 10^{-9.5}$ obtained in [94] is actually much weaker (for a more detailed discussion of this constraint, see [88]).

$$\mathrm{Br}(o\text{-Ps} \longrightarrow \textit{invisible}) < 10^{-5}. \quad (53)$$

The first experiment on the o-Ps $\longrightarrow$ *invisible* decay, motivated by a puzzle in the o-Ps decay rate, was performed a long time ago [65] and then repeated with higher sensitivity [63]. The results exclude contributions to the o-Ps decay rate from invisible decay modes (such as o-Ps $\longrightarrow \nu\nu$, millicharged particles, etc.) at the level of $\mathrm{Br}(o\text{-Ps} \longrightarrow \textit{invisible}) < 3 \times 10^{-6}$, but are not very sensitive to the o-Ps $\longrightarrow$ o-Ps' oscillation mechanism because of the high collision rate in these experiments. Indeed, the limit on ϵ extracted from the results of [63], taking into account the suppression collision factor, is $\epsilon < 10^{-6}$ [90] and is not strong enough to exclude a possible mirror-matter contribution at a level comparable with the BBN limit of Eq. (52). Hence, it is absolutely fundamental to distinguish experiments in "vacuum," where o-Ps is contained, for example, in a large evacuated cavity, from other setups where o-Ps undergoes numerous interactions with the environment within its lifetime. Future experiments, which might shed light on this issue, are discussed in Section 5.

How does the picture of mirror matter as a dark matter candidate fit into the global picture of the evolution of the Universe as predicted by cosmology? Berezhiani [82] brought up important points concerning these issues: naively, mirror parity implies that ordinary and mirror sectors should have the same cosmology, and so ordinary and mirror particles should have the same cosmological densities. However, this would be in immediate conflict with the Big Bang nucleosynthesis (BBN) bounds on the effective number of extra light neutrinos. Therefore, the mirror particle density in the early Universe should be appropriately reduced. This situation is plausible if the following conditions are satisfied [82]:

(a) at the Big Bang, the two systems are born with different densities;

(b) the two systems interact very weakly, so that they do not come into the thermal equilibrium with each other in the early Universe;

(c) both systems expand adiabatically, and there is no significant entropy production at the later times which could heat the mirror sector and equilibrate its temperatures to the ordinary one.

Because of the temperature difference, in the mirror sector, all key epochs, such as the baryogenesis, nucleosynthesis, etc. proceed at somewhat different conditions than in the observable universe. In particular, in certain baryogenesis scenarios, the mirror world generically should get a larger baryon asymmetry than the ordinary sector, and it is quite plausible that the dark matter of the Universe, or at least its significant fraction is constituted by mirror baryons, which are obviously dark for the ordinary observer [95].

4.3. New Light X Boson

Consider now *the model with a light vector X boson* and with the interaction $L_I = g_X X^\mu \bar{\psi}\gamma_\mu\psi$, which also leads to invisible decay of o-Ps.[8] Suppose, in addition, that X boson interacts with other particles (fermions) or (as a consequence of the Higgs mechanism) with itself and the scalar field. The contribution of the X boson into electron anomalous magnetic moment is given by the well-known formula

$$\delta a_e = \frac{\alpha_{Xe}}{\pi}\int_0^1 \frac{x^2(1-x)}{x^2 + (1-x)\dfrac{m_X^2}{m_e^2}}, \quad (54)$$

where $\alpha_{Xe} = \dfrac{g_X^2}{4\pi}$. For $m_X \ll m_e$, from the bound on anomalous electron magnetic moment, one can find [8] that $\alpha_{Xe} < 3 \times 10^{-10}$. For the opposite case of heavy X boson ($m_X \gg m_e$), the bound on the anomalous electron magnetic moment leads to the bound [8]

$$\alpha_{Xe}\frac{m_e^2}{m_X^2} < 4.5 \times 10^{-10}. \quad (55)$$

For the reaction o-Ps $\longrightarrow X^* \longrightarrow X_1\bar{X}_1$ (here, X^* is virtual X-boson and X_1 is a fermion (sterile neutrino) or a scalar particle), one can find that

$$\mathrm{Br}(o\text{-Ps} \longrightarrow X^* \longrightarrow X_1\bar{X}_1) = \frac{3\pi}{4(\pi^2-9)} kF\left(\frac{m_{X_1}^2}{m_e^2}\right)\left(1 - \frac{m_{X_1}^2}{m_{0\text{-Ps}}^2}\right)^{-2}\frac{\alpha_{Xe}\alpha_{XX_1}}{\alpha^3}, \quad (56)$$

where $F(x) = \left(1 - \dfrac{x}{2}\right)(1-x)^{1/2}$, $k = 1$ for spin $\dfrac{1}{2}$ and $F(x) = (1-x)^{3/2}$, $k = \dfrac{1}{4}$ for spin 0, $\alpha_{XX_1} = g_{XX_1}^2/4\pi$. For $m_X \ll m_e$, we find [8] that

$$\mathrm{Br}(o\text{-Ps} \longrightarrow X^* \longrightarrow X_1\bar{X}_1) \le k \times 2 \times 10^{-3}\alpha_{XX_1}. \quad (57)$$

To have experimentally interesting branching, say of the order $O(10^{-6})$, for $\alpha_{Xe} = 3 \times 10^{-10}$, we must have $\alpha_{XX_1} \sim 5 \times 10^{-4}$, which looks reasonable. In the opposite limit $m_X \gg m_e$, the corresponding bound reads

$$\mathrm{Br}(o\text{-Ps} \longrightarrow X^* \longrightarrow X_1\bar{X}_1) \le k \times 3 \times 10^{-3}\alpha_{XX_1}\frac{m_e^2}{m_X^2}. \quad (58)$$

[8] For the recent phenomenological bounds in models with light vector X-boson related to the muon $(g-2)$ and so-called NuTeV anomaly, see [8, 96, 97] and also [98].

For X-boson mass close to the orthopositronium mass, we have the enhancement factor $\left(1-\frac{m_X^2}{m_{o\text{-Ps}}^2}\right)^{-2}$ in formula (41) for the branching ratio, and, hence, the coupling constants $\alpha_{\mathrm{Xe}}\alpha_{XX_1}$ could be smaller. It should be noted that we can treat X boson as a mirror orthopositronium which, due to the mixing of our photon with a mirror photon, has direct coupling with electrons and decays into three invisible mirror photons. Vector boson X acquires a mass via the Higgs mechanism, and, for both light X boson and the Higgs scalar ϕ, the reaction ("Higgs–Strahlung" process)

$$o\text{-Ps} \longrightarrow X^* \longrightarrow X\phi \tag{59}$$

also leads to invisible o-Ps decay mode. The corresponding formula for the o-Ps branching in the limit $m_x \ll m_e$, $m_\phi \ll m_e$ coincides with formula (41) for $k = \frac{1}{4}$ (scalar case) and leads to a similar bound on the product $\alpha_{\mathrm{Xe}}\alpha_{X\phi}$.

4.4. Extra Dimensions

Recently, *the models with infinite additional dimensions* of Randall–Sundrum type (brane-world models) [99, 100] have become very popular. There is a hope that models with big compactification radii [99–103] will provide the natural solution of the gauge hierarchy problem. For instance, as has been shown [99] on the example of the five-dimensional model, there exists a thin-brane solution to the five-dimensional Einstein equations which has flat four-dimensional hypersurfaces,

$$ds^2 = a^2(z)\eta_{\mu\nu}dx^\mu dx^\nu - dz^2. \tag{60}$$

Here,

$$a(z) = \exp(-k(z-z_c)), \tag{61}$$

and the parameter $k > 0$ is determined by the five-dimensional Planck mass and bulk cosmological constant. For the model with metric (40), the effective four-dimensional gravitational constant is

$$G_{(4)} = G_{(5)}k\frac{1}{\exp(2kz_c)-1}. \tag{62}$$

One can solve the gauge hierarchy problem in this model if $k \sim M_{EW} = 1$ TeV, $G_{(5)} \sim k^{-3}$. As it follows from expression (42), the Planck scale in this model is

$$M_{PL} \sim \exp(kz_c)M_{EW}, \tag{63}$$

which means the existence of exponential hierarchy between Planck and electroweak scales. For $z_c \approx 37k^{-1}$, we have correct quantitative relation among Planck and electroweak scales. Note that, in this model, the mass of the first gravitational Kaluza–Klein state is $m_{\mathrm{grav}} \sim k$. As has been shown in [104], in this model, the massive matter becomes unstable due to a tunneling effect and disappears into the additional fifth dimension. For massive scalar particle Φ with the mass m, the transition rate into the additional dimension is given by the formula [104]

$$\Gamma(\Phi \longrightarrow \text{additional dimension}) = \frac{\pi m}{16}\left(\frac{m}{k}\right)^2. \tag{64}$$

It should be stressed that o-Ps is a good candidate for the search for the effect of the disappearance into additional dimension(s) [105], since it has specific quantum numbers similar to those of vacuum and is a long-lived system. This might enhance the probability of the transition. For massive vector particles, the expression for its transition rate into additional dimension(s) is not explicitly known. To make quantitative estimates, we shall use formula (49) for the decay width of spin-1 particle. For the orthopositronium invisible decay into additional dimension(s)

$$o\text{-Ps} \longrightarrow \gamma^* \longrightarrow \text{additional dimension(s)}, \tag{65}$$

the corresponding branching ratio is

$$\mathrm{Br}(o\text{-Ps} \longrightarrow \gamma^* \longrightarrow \text{additional dimension(s)}) = \frac{9\pi}{4(\pi^2-9)}\frac{1}{\alpha^2}\frac{\pi}{16}\left(\frac{m_{o\text{-Ps}}}{k}\right)^2 \approx 3\times 10^4\left(\frac{m_{o\text{-Ps}}}{k}\right)^2. \tag{66}$$

The important bound on the parameter k [105] arises from LEP1 data on $Z \longrightarrow$ *invisible* decay, namely $k \geq 2.7$ TeV [105]. Using this bound, we find that

$$\mathrm{Br}(o\text{-Ps} \longrightarrow \text{additional dimension(s)}) \leq 4\times 10^{-9}. \tag{67}$$

To solve the gauge hierarchy problem, models with additional infinite dimension(s) must have the $k \leq O(10)$ TeV. This means that

$$\mathrm{Br}(o\text{-Ps} \longrightarrow \text{additional dimension(s)}) \geq O(10^{-10}). \tag{68}$$

Since these estimates give only a correct order of magnitude for the lower and upper limits on corresponding branching ratio, we believe that region of $\mathrm{Br}(o\text{-Ps} \longrightarrow \textit{invisible}) \approx 10^{-9}$–$10^{-8}$ is of great interest for observation of the effect of extra dimensions.

Thus, we saw that the invisible decay of orthopositronium may occur at a rate within several (two or three) orders of magnitude of the present experimental upper limit. We believe that this enhances other motivations and justifies efforts for the more sensitive search for o-Ps $\longrightarrow$ *invisible* decay to be done in a near future experiment described below in Section 6.1.

5. NEW SEARCHES FOR INVISIBLE DECAY OF ORTHOPOSITRONIUM

As already mentioned in the previous section, the new models that are relevant to the o-Ps $\longrightarrow$ *invisible* decay mode predict the existence either of (i) extra

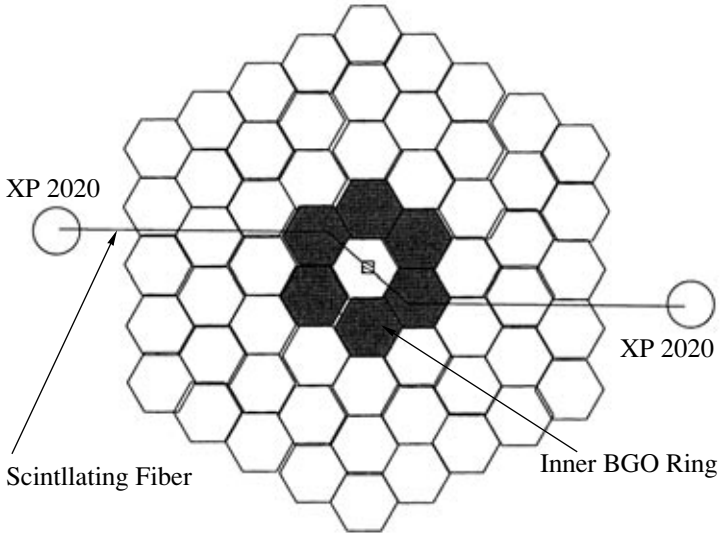

Fig. 4. Schematic illustration of the ETHZ–INR experimental setup. Positrons from the ^{22}Na source deposited on the central part of the scintillator fiber stop in the SiO_2 target (dashed area in the center) and form *o*-Ps atoms. The target is surrounded by a hermetic γ-detector, which consists of ~100 BGO crystals viewed by the photomultipliers.

dimensions, (ii) fractionally charged particles, (iii) a new light vector gauge boson, or (iv) dark matter of the mirror matter type. The required sensitivity in the branching ratio Br(*o*-Ps $\longrightarrow$ *invisible*) for the possible observation of these phenomena has to be at least as low as 10^{-8}.

5.1. The ETH–INR Experiment with the SiO_2 Target

A new experiment, aimed at developing a 4π hermetic calorimeter with an extremely low photon detection inefficiency was recently proposed [107]. The schematic illustration of the experimental setup is shown in Fig. 4. The main components of the detector are the positron source (^{22}Na), the positron tagging system composed of a scintillating fiber viewed by two photomultipliers (PM), the positronium formation SiO_2 target, and a hermetic γ-detector.

The coincidence of the PM signals from the positrons crossing the fiber opens the gate for the data acquisition (DAQ). In the offline analysis, the 1.27 MeV photon, which is emitted from the source simultaneously with the positron, is required to be in the trigger BGO counter resulting in a high confidence level of positron appearance in the positronium formation region. A positron which enters the SiO_2 target may capture an electron, creating positronium. The calorimeter detects either the direct 2γ annihilation in flight or the two (three) photons from the para- (ortho-)positronium decays in the target. The occurrence of the *o*-Ps $\longrightarrow$ *invisible* decay would appear as an excess of events with deposition in the calorimeter compatible with zero above those expected from the Monte Carlo prediction or from the direct background measurement. This measurement presents a new feature of this type of experiment. The idea is to obtain a pure *o*-Ps decay energy spectrum by comparing two different spectra from the same target filled either with N_2 (low *o*-Ps quenching rate) or with air, where the presence of paramagnetic O_2 will quench the fraction of *o*-Ps in the target from 10% down to 3% due to the spin exchange mechanism:

$$o\text{-Ps} + O(\uparrow\uparrow) \longrightarrow p\text{-Ps} + O(\downarrow\uparrow). \qquad (69)$$

Thus, the subtraction of these properly normalized spectra will result in a pure *o*-Ps annihilation energy spectrum in the γ-detector. The experiment is currently in the commissioning phase (see Fig. 5).

5.2. The Berkeley–LLNL Experiment

A collaboration at Lawrence Berkeley and Lawrence Livermore National Laboratories is investigating the feasibility of extending the sensitivity of such an experiment to the level of 10^{-9}. The primary idea is to use a large volume of liquid organic scintillator as a hermetic γ-detector, e.g., similar to the design of the KamLAND neutrino experiment [12]. Elementary calculations suggest that such a detector would require a roughly 3 m diameter in order for there to be a negligible probability for two 511 keV photons to each leave less than ≈100 keV of energy in the detector volume. The total mass of such a volume of liquid scintillator would be roughly 10^5 kg. Several options for the positron source, such as the ^{22}Na source, short-lived light isotopes, and even clean positron beam are considered. The *o*-Ps formation target is supposed to be the silica aerogel. One limitation is the counting time required to observe roughly 10^9 Ps formation triggers, while allowing a several-microsecond observation window to allow the *o*-Ps component to decay away such

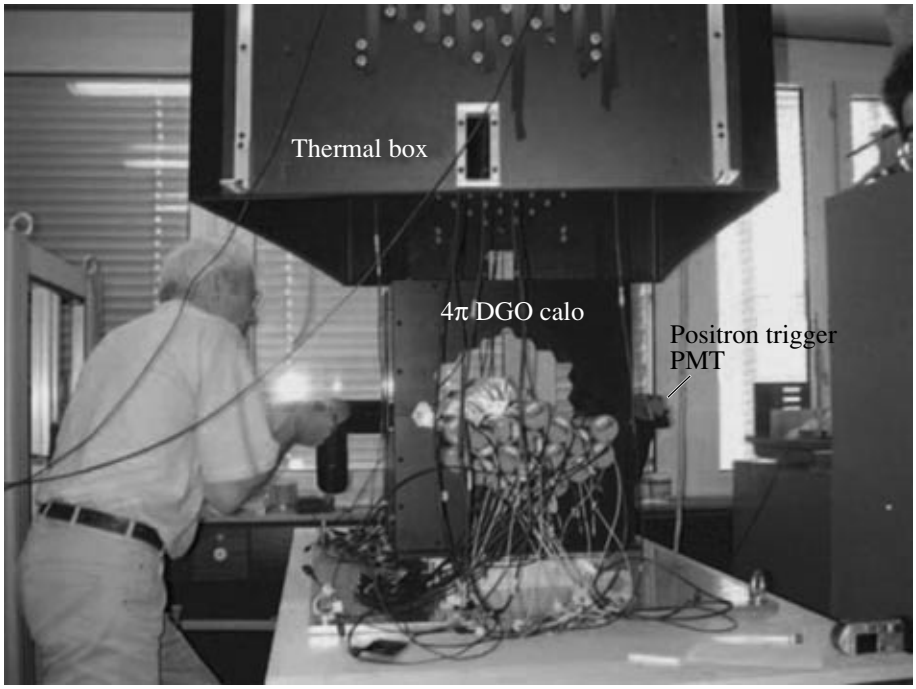

Fig. 5. ETHZ–INR experiment for *o*-Ps ⟶ *invisible* decay search in silica aerogel.

that the exponential decay probability is less than the desired branching ratio. In such a case, the accidental rate should not give an appreciable probability that a second decay would occur. Such a geometry naturally addresses the hermeticity requirement, but the sacrifice in compactness and larger mass compared to an array of high-Z inorganic solid scintillators is clear. In such an experiment, the greatest challenge seems to be to provide as clean a trigger as possible for the positron appearance.

5.3. The ETH–INR Vacuum Experiment

The concepts for a new experiment, designed with the goal of observing the *o*-Ps ⟶ *invisible* decays, if the branching ratio is greater than 10^{-7}, were presented in [108]. Figure 6 shows a schematic view of the experimental setup.

Accordingly, the apparatus is designed with several distinct parts: (i) a pulsed slow positron beam [109, 110] and a low-mass target for efficient orthopositronium production in a vacuum chamber; (ii) a positron appearance tagging system with a high signal-to-noise ratio based on a high-performance MCP; and (iii) an almost 4π BGO crystal calorimeter (ECAL) surrounding the vacuum chamber for efficient detection of annihilation photons. The chamber has as little wall mass as possible to minimize photon energy absorption. The target is supposed to be made of a special thin film of porous SiO_2, where *o*-Ps is formed with ~30% efficiency (see Section 8, Fig. 16). *o*-Ps's thermalized due to the high collisional rate are able to diffuse through the pore network over distances much longer than the film thickness and escape through the film surface into vacuum [111]. The Monte Carlo simulations show that the collisional rate of *o*-Ps's with the vacuum chamber walls is expected to be less than a few collisions per *o*-Ps lifetime [108].

The occurrence of the *o*-Ps ⟶ *o*-Ps' ⟶ *invisible* conversion would appear as an excess of events with energy deposition comparable with zero in the calorimeter above those expected from the prediction of the background. In case of a signal observation, the number of excess events could be crosschecked by small variations of experimental conditions which affect the *o*-Ps ⟶ *o*-Ps' transition rate but do not result in a loss of energy from ordinary positron annihilations. The identification of signal events relies on the high-efficiency measurement of the energy deposition from the annihilation of positrons.

To achieve a sensitivity in the branching ratio of 10^{-7} in a reasonable amount of data-taking time, the rate of *o*-Ps decays per second has to be as high as possible, consistent with minimal reduction of the *o*-Ps ⟶ *invisible* signal efficiency and acceptably small dead time. The trigger rate in the photon detector is expected to be $\simeq$100 Hz, which is low enough to allow these events to be recorded without losses, and is high enough to reach the expected sensitivity (see below) in a reasonable time.

Positrons from the pulsed beam are stopped in the target and either form positronium, i.e., *o*-Ps or *p*-Ps, or annihilate promptly into 2γ's. The secondary electrons (SE) produced by the positrons hitting the target are

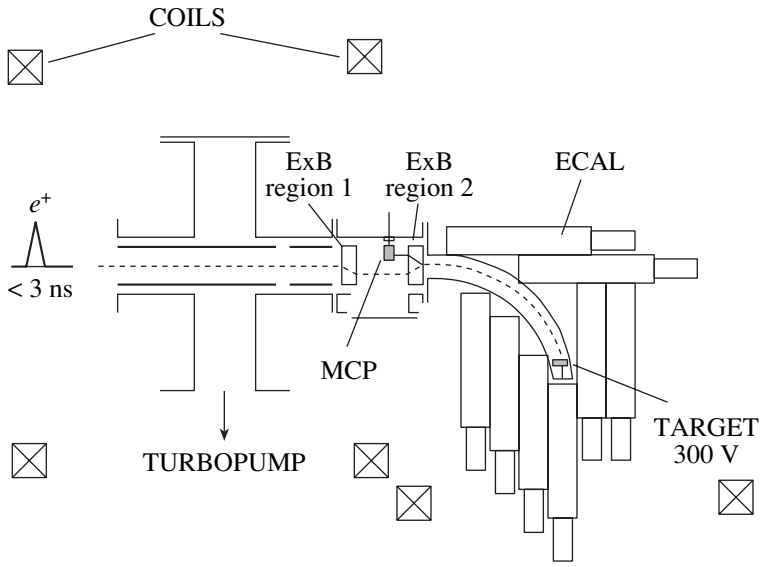

Fig. 6. Schematic diagram of the ETH–INR experimental setup. Upstream of the $E \times B$ region *1*, the drift tube 4 of the pulse beam shown in Fig. 7 is located. The ECAL is composed of BGO counters viewed by photomultipliers.

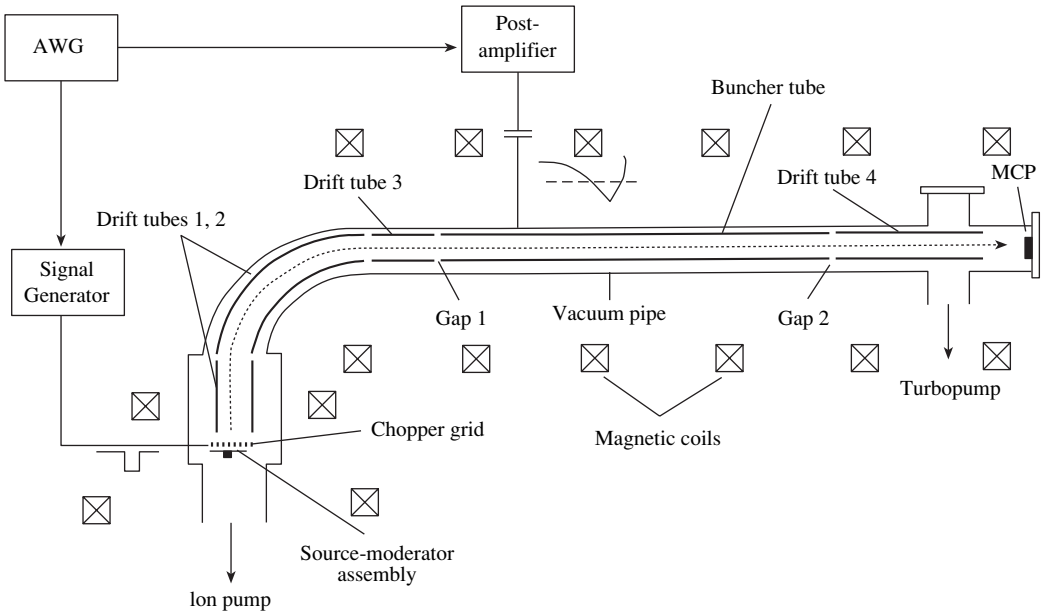

Fig. 7. Schematic illustration of the magnetically transported pulsed positron beam.

accelerated by the voltage applied to the target relative the grounded transport tube. Then they are transported by a magnetic field in the backward direction relative to the positrons moving in spirals along the magnetic field lines and deflected to a microchannel plate (MCP) by a $E \times B$ filter.

The trigger for data acquisition is generated by a coincidence within ±3 ns of a pulse from the MCP and the signal from the pulsed beam, which is synchronized with the positron arrival time at the target.

It is hoped that the beam can serve several different experiments. Thus, the final beam construction should compromise several design goals, which are summarized as follows:

beam energy range from 100 to 1000 eV;

beam intensity of $\simeq 10^4$–10^5 positrons per second;

pulse duration at the target $\delta t_T < 3$ ns for an initial pulse duration at the moderator $\delta t_M \simeq 300$ ns;

repetition rate 0.3–1.0 MHz;

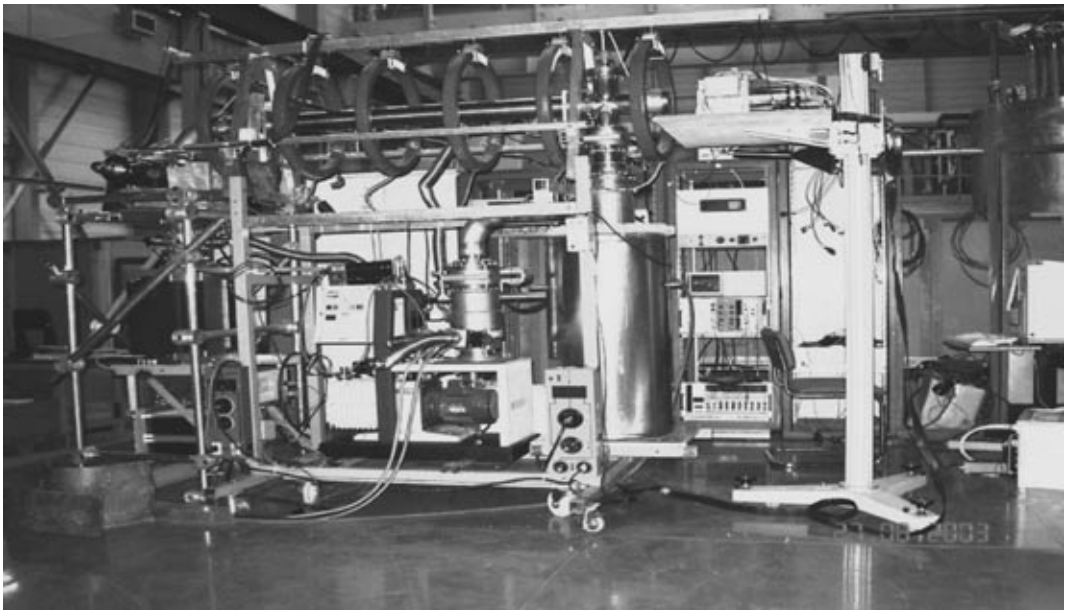

Fig. 8. Photograph of the ETH–INR slow positron pulsed beam prototype.

peak/noise ratio ~10^2, (single) Gaussian shape of the pulse;

beam spot size at the target position is of the order of a few millimeters assuming 3–5 mm ^{22}Na source diameter.

The first measurement results obtained with the constructed pulse positron beam are reported in Section 6.

The experimental signature of the o-Ps $\longrightarrow$ *invisible* decay is an excess of events above the background at zero-energy deposition in the ECAL. The 90% confidence level limit on the branching ratio for the o-Ps $\longrightarrow$ *invisible* decay for a background free experiment is given by

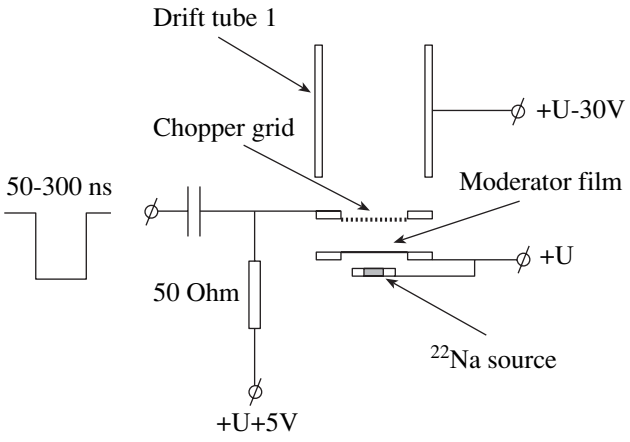

Fig. 9. Schematic illustration of the source–moderator assembly.

$$S(90\%) = \frac{N(o\text{-Ps} \longrightarrow \textit{invisible})}{N_{o\text{-Ps}} N_{\text{coll}}}, \qquad (70)$$

where $N(o\text{-Ps} \longrightarrow \textit{invisible}) = 2.3$ and the terms in the denominator are the integrated number of produced o-Ps's ($N_{o\text{-Ps}}$) and the average number of o-Ps collisions in the chamber, respectively. The number $N_{o\text{-Ps}}$ is defined as a product $N_{o\text{-Ps}} = R_{e^+}\epsilon_{o\text{-Ps}}\epsilon_{e^-}t$, where the first factor is the number of delivered positrons per second on the target, the second one is the efficiency for o-Ps production, and the third one is the efficiency of the secondary electron transportation from the target to the MCP in the positron tagging system. Taking $R_{e^+} = 2 \times 10^3$ s^{-1}, $\epsilon_{o\text{-Ps}} = 20\%$, and $\epsilon_{e^-} = 100\%$, we expect $\approx 7 \times 10^7$ prompt and $\approx 1.7 \times 10^7$ o-Ps annihilations per day. Thus, $S(90\%) \simeq 10^{-7}$.

In case of the observation of zero-energy events, one of the approaches would be to measure their number as a function of the residual gas pressure in the chamber. This would allow a good crosscheck: relatively small variations of gas pressure results in larger peak variations at zero energy due to the damping of o-Ps $\longrightarrow$ o-Ps' oscillations.

5.4. The LEPTA Experiment

The new low-energy positron/electron storage ring LEPTA [112], originally discussed in [113], is dedicated to the construction of a small positron storage ring with electron cooling of positrons circulating in the ring [114]. Such a peculiarity of this facility enables it to be an efficient generator of orthopositronium atoms

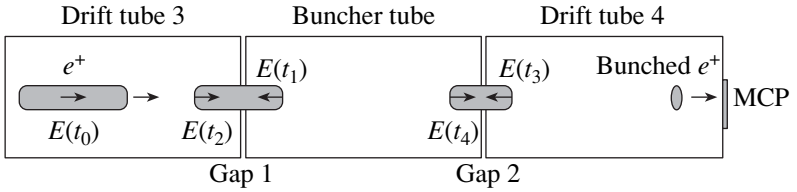

Fig. 10. Principle of the positron beam compression with a double gap buncher: at the time t_0, all chopped positrons have received initial acceleration; at the time $t_1 > t_0$ ($t_3 > t_2$), positrons passing the first (second) gap early are decelerated, while those which pass the gap at a later time $t_2 > t_1$ ($t_4 > t_3$) are accelerated. After this velocity modulation, positrons arrive at the target position (MCP) as a short bunch.

[115]. The creation of slow *o*-Ps beam opens up many interesting possibilities to probe new physics beyond the SM with positronium. For example, a sensitive test of the *CPT*-invariance and the fundamental law of the electric charge quantization could be performed by the direct comparison of the electric charges of the particles forming *o*-Ps atoms by measuring their displacement after crossing a transverse magnetic field [117]. The LEPTA group has also discussed the possibility of searching for the *o*-Ps $\longrightarrow$ *invisible* decay in vacuum. The proposed method is based on the measurements of the dependence of the *o*-Ps decay rate on coordinate *X* along the vacuum channel, where the *o*-Ps flux travels (see, e.g., [118]).

The analysis of the systematic errors shows that this experiment could be sensitive to the Br(*o*-Ps $\longrightarrow$ *invisible*) as low as $\sim 10^{-6}$, resulting in the sensitivity to the mixing strength $\epsilon \sim 10^{-8}$ [116]. The new independent experiment with the sensitivity in the Br(*o*-Ps $\longrightarrow$ *invisible*) below the BBN limit of Eq. (53) would be very interesting and important.

6. PULSED SLOW POSITRON BEAM

For the ETH–INR vacuum experiment discussed above, a specially designed slow positron beam operating in a pulsed mode with a repetition period $\simeq 1$ μs has been constructed. The construction of the beam has to compromise two main design goals [119]: (i) the time of the primary positron collection has to be comparable with the pulsing period in order to get the highest pulsing efficiency (the ratio of beam intensities in the pulsed and dc modes) and to enhance the signal-to-noise ratio; (ii) a high beam compression factor of $\simeq 100$ has to be achieved in order to obtain a positron pulse width of a few ns and to suppress background for tagging of *o*-Ps production.

Various techniques to produce pulsed positron beams have been reported, with the main focus so far on material science applications (for a review, see, e.g., [127, 129]). The Munich [120] and the Tsukuba [121] groups use a sinusoidal RF field in the pulsed beam formation. They have achieved bunch pulse widths of 0.2–0.3 ns for an initial pulse duration of 5–15 ns. For the vacuum experiments mentioned above, this method requires a wide time window of chopping, and, accordingly, the positron collection efficiency from an initial dc beam becomes less than 1%.

A pulsing system based on another method has recently been considered by Oshima et al. [122]. The main idea is the same as for the RF method: the time of flight for each positron is adjusted according to the time it arrives at the starting point of acceleration. However, instead of applying a sinusoidal RF field, a more suitable pulse shape of the electric field is generated, such as an approximate inverse parabolic function of time [123]. This method has been further developed by Iijima et al. [124] for measurements in which the lifetime of orthopositronium atoms is close to its vacuum value of $\simeq 142$ ns. For these applications, it is necessary to modify the originally proposed technique in order to generate higher-intensity positron beams by accumulating positrons over a wider time interval, even though the bunch width becomes larger, but still much less than the typical measured timing intervals of $\simeq 100$ ns. Using a high permeability buncher core, a bunch width of 2.2 ns (FWHM) for 50 ns collection time and a repetition period of 960 ns have been achieved [124]. One of the problems encountered is the limitation of the voltage supplied by a postamplifier to the buncher. In this section, we describe the new recently constructed pulsed slow positron beam [125] based on the use of a double-gap coaxial buncher powered by an RF pulse of

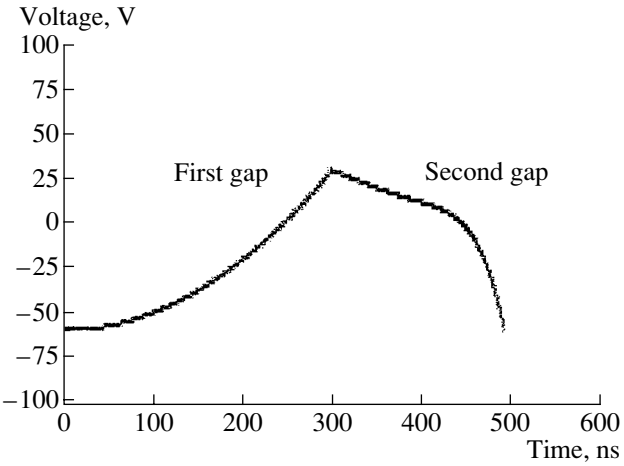

Fig. 11. The bunching voltages seen by the positrons at the first and the second velocity modulation gaps, respectively.

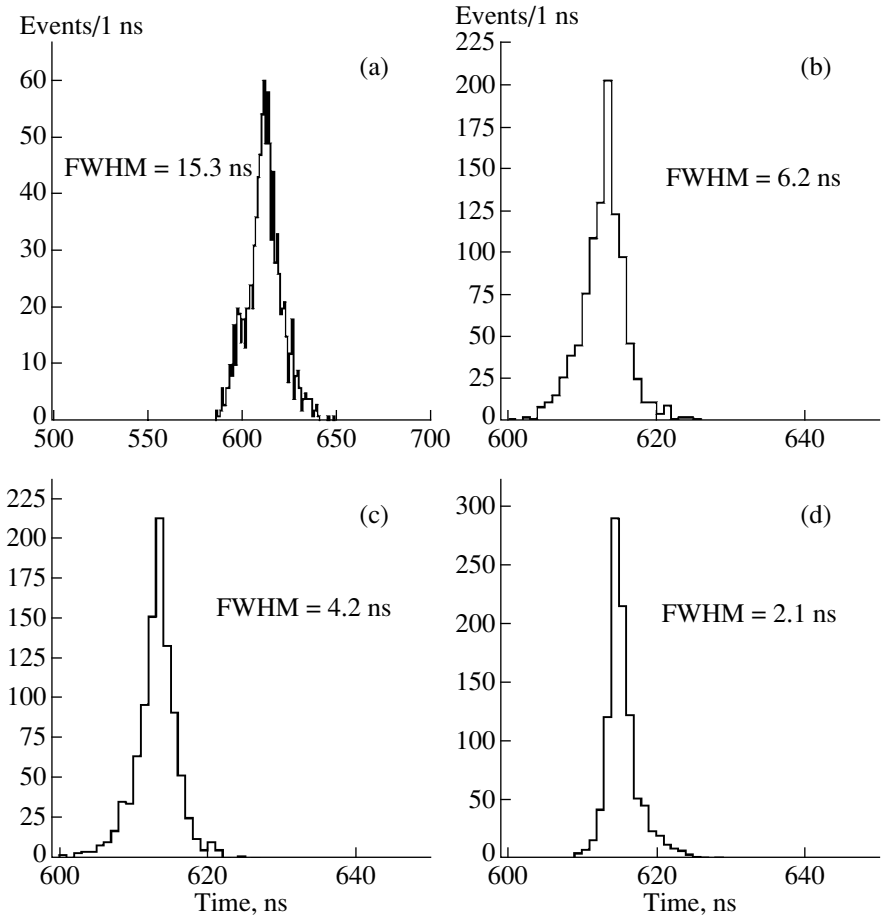

Fig. 12. Simulated time distributions of bunched positrons at the MCP for an initial chopped pulse of 300 ns. The cuts on the longitudinal energy $E_{\|}$ of positrons emitted from the moderator are: (a) >0 eV, (b) >1.5 eV, (c) >2.0 eV, and (d) >2.5 eV. The initial positron energy distribution is taken from the measurements shown in Fig. 13b; the angular distribution is taken to be isotropic.

appropriate shape, which is produced by an arbitrary waveform generator (AWG) and by a postamplifier. This pulsing method allows to reduce the influence of aberrations of the bunching pulse shape in comparison with methods using a sinusoidal RF voltage and to achieve a compression ratio limited mainly by the intrinsic energy spread of the initial positrons. In comparison with the one-gap buncher method (see, e.g., [122]), the present scheme requires lower bunching voltage and less postamplifier power.[9]

6.1. The Pulsed Slow Positron Beam

6.1.1. The actual beam. The preliminary design of the present pulsed slow positron beam has been reported in [119]. Our primary consideration is that the system should be of the magnetic transport type, because this provides the simplest way to transport a slow positron beam from the positron source to its target [126–130]. Figures 7 and 8 show the schematic illustration of the developed pulsed slow positron beam and the photograph of the actual beam, respectively.

The DC slow positrons are produced by moderation of fast positrons emitted from β^+-decays of the radioisotope source ^{22}Na. This source, with a relatively small activity (~50 μCi) was prepared by bombarding a 150 μm thick foil of pure Al with a 690 MeV proton beam at the PSI accelerator (Paul Scherrer Institute, Switzerland). The moderator, a tungsten W(100) single crystal foil with a thickness of 1 μm, is prepared in situ by annealing it at 2000°C (see Section 4). A few eV positrons from the moderator are accelerated to 30 eV and are separated from the fast unmoderated positrons by a 90° curved *B*-field, serving as a velocity filter. The eight coils provide a quasiuniform longitudinal magnetic field of 70 G to guide positrons down to the target—a microchannel plate (MCP, Hamamatsu F4655-12) located at the end of the beam line and used for positron detection. The beam energy can be varied up to a few kV simply by applying to the beam drift tubes the desired electrostatic potentials.

[9] More details on a pulsing system with a single-gap velocity modulation can be found in [122, 123].

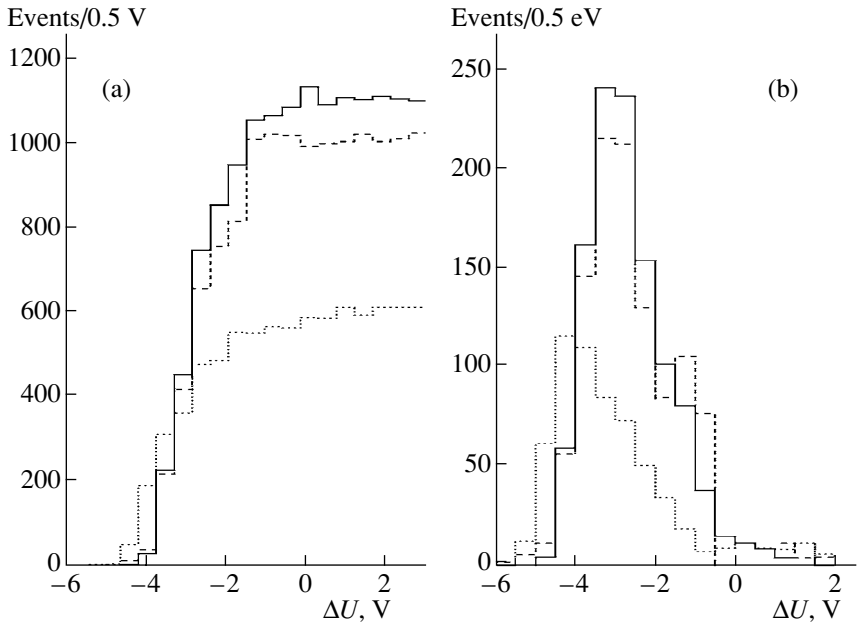

Fig. 13. (a) Positron yield as a function of the potential difference between the moderator and chopper grid; (b) longitudinal kinetic energy distribution of moderated positrons for the W(100) single crystal, moderated before (dotted), ~1 h after (solid), and 2 days after (dashed) in situ annealing.

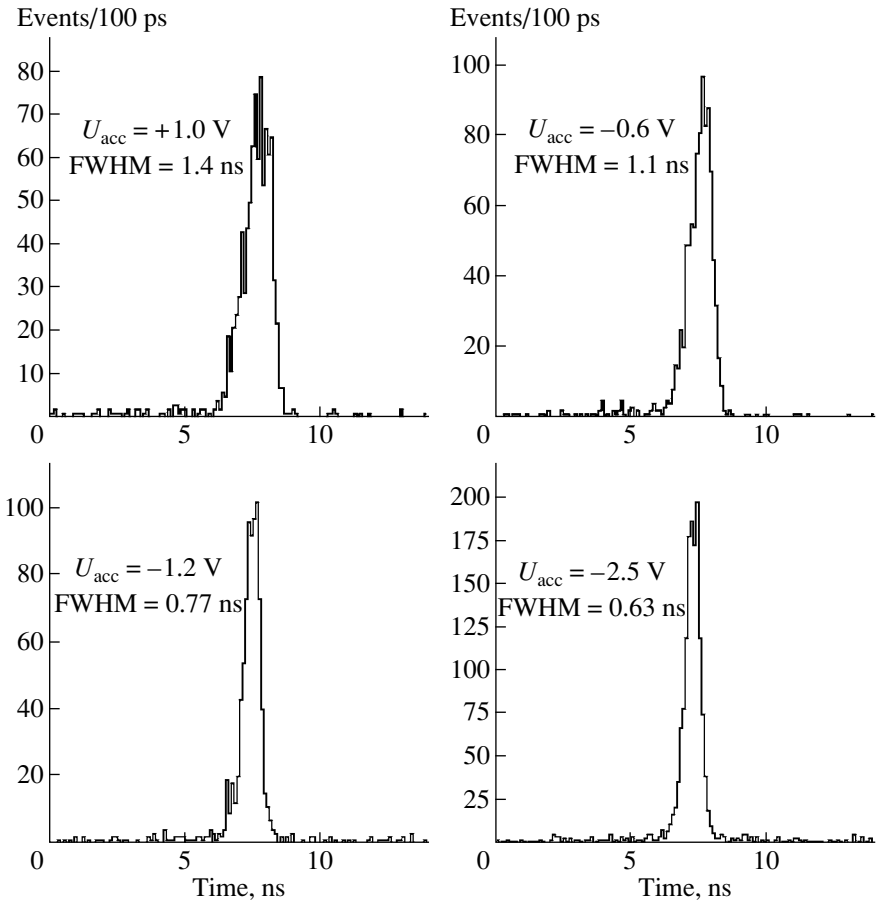

Fig. 14. Time distributions of pulsed positrons at the target position, measured for an initial positron pulse of 90 ns and for different potential difference U_{acc} between the moderator and the grid indicated on the plots.

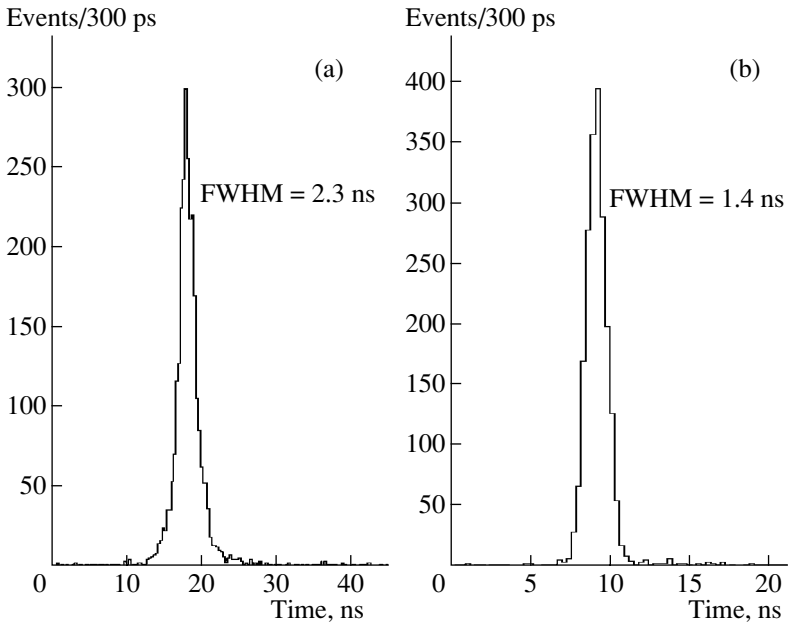

Fig. 15. Measured time distribution of pulsed positrons at the target position for an initial pulse duration of (a) 300 ns and (b) 120 ns, respectively.

The positron pulsing section shown in Fig. 7 consists of a chopper, two drift tubes, and a buncher. The latter is constructed in such a way that its internal tube (the buncher electrode) forms a coaxial line of 50 Ω impedance with the external vacuum pipe. The buncher length (~150 cm) is determined by the distance-of-flight of positrons entering the buncher during the initial pulse and by their energy. For the initial pulse of 90 ns, the repetition period can be varied from ≃100 ns to infinity. Initial positron pulses with the desired duration are formed with the chopper grid placed 4 mm downstream of the moderator foil. The potential difference U_{acc} = 5 V between the grid and the moderator foil is used for repelling the slow ≃3 eV positrons emitted from the moderator (see Fig. 9). When the chopper pulse of a given duration (50–300 ns) and a rectangular shape, produced by a standard fast-signal generator, is applied to the grid with an amplitude of about 5 V, the moderated positrons come through and are accelerated in the gap between the chopper grid and the first drift tube.

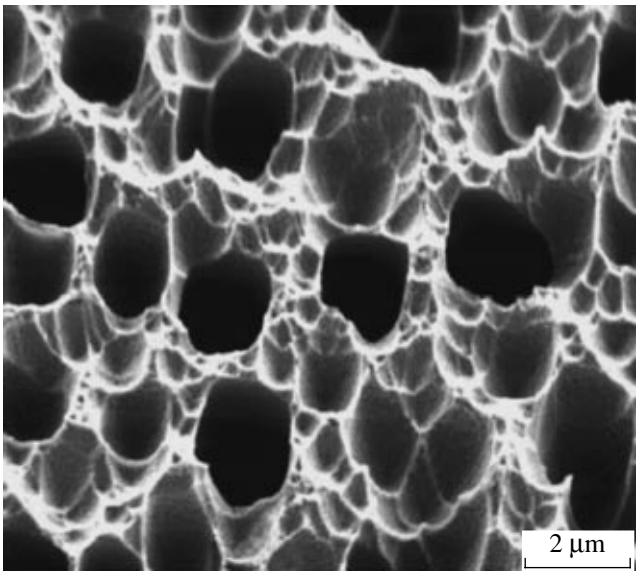

Fig. 16. An example of a porous SiO_2 film [143] top viewed by SEM. The 2 μm scale is shown to evaluate the pore sizes of the sample.

6.1.2. The pulsing scheme for the buncher. The principle of the positron pulsing method is illustrated in Fig. 10. A nonlinear time-varying electric field in the first gap (Gap 1) between the drift tube 3 and the bunching electrode modulates the velocity of positrons in such a way that those (initially chopped and accelerated) positrons which arrive earlier are decelerated at the gap, while those which reach the gap later are accelerated. In the second gap (Gap 2) between the buncher and drift tube 4, the same procedure is repeated. The chopper pulse is synchronized with the AWG trigger signal such that the chopped initial positrons passing the bunching electrode receive the correct bunching voltage from the corresponding part of the bunching pulse. Finally, the initially chopped positron pulse arrives at the MCP target as a bunch of small width.

The bunching voltage of the designed shape is produced by the arbitrary waveform generator (AWG-510, Tektronix). The AWG output pulse is then amplified by the postamplifier 100A250A (Amplifier Research) and is applied to the bunching electrode. The amplifier has

an output power of 100 W and a bandwidth of 10 kHz–250 MHz, allowing it to drive the 50 Ω coaxial buncher with a pulse amplitude up to ≃80 V without saturation. The time profile of the bunched positrons at the MCP position is measured by using the MCP signal as the TDC–START and the AWG signal as the STOP; the STOP signal is also used to trigger the chopper pulse.

6.2. Design of the Pulsing System

The simulations of the *E*, *B*-fields, extraction optics, the beam transport, and the velocity modulation of positrons are performed with the GEANT4 [131] and 3D-Bfield [132] codes with the goal of minimizing the time width of the bunch and optimizing the shape of the bunching pulse.

The optimal shape and duration of the bunching pulse was calculated for the given initial positron pulse duration by taking into account the following criteria:

the amplitude of the RF bunching pulse should be within ±80 V;

after the velocity modulation, positrons should arrive at the target as a bunch within a time spread of ≃1 ns;

absence of significant nonlinear distortions of the beam phase space at the target position.

For the first gap and for an initial pulse of, e.g., 300 ns, a parabolic time-varying potential $V(t) \sim t^2$ changing from –60 V (decelerating part) to +30 V has been chosen, as shown in Fig. 11. The time dependence of the potential at the central electrode of the buncher at times $t > 300$ ns can then be calculated, solving the corresponding equations with an iterative procedure under the condition that positrons arrive at the target simultaneously and that the potential at the electrode at the end of the bunching pulse returns to its initial value –60 V. In Fig. 11, the resulting shape of the bunching voltage is shown for both gaps.

In reality, the bunching pulse shape differs from its ideal theoretical shape, mostly due to the finite-frequency bandwidth of the postamplifier and due to nonideal matching of the coaxial buncher circuit to 50 Ω impedance. To estimate the effect, the response of the 100A250A amplifier was simulated according to its circuit characteristics [133]. The residual shape is defined as $R(t) = S_{out}(t) - S_{in}(t)$, where $S_{in}(t)$ is the input signal supplied by the AWG with unit amplitude and $S_{out}(t)$ is the amplifier output pulse calculated for unit gain.

It was found that, for an initial pulse duration of 300 ns, the deviation of the response from the ideal shape shown in Fig. 11 is not more than about $R(t)/S_{out} \simeq \pm 1\%$ over the full bunching pulse duration. The simulations show that a signal deviation of 1% does not result in a significant distortion of the bunched positron pulse shape. The FWHM of the corresponding distribution has been increased by less than 2%. However, for shorter initial pulses (<100 ns), deviations up to $R(t)/S_{out} \simeq \pm 5\%$ have been observed. This will result in a significant degradation in the FWHM and shape of the positron pulses. These results mean that the theoretical shape of the bunching pulse must be reproduced within about ±1% precision. For an initial positron pulse duration of more than ≃100 ns, this value is achievable.

In Fig. 12, simulated time distributions of bunched positrons at the target are shown for different cuts on the longitudinal kinetic energy $E_{\|}$ of positrons emitted from the moderator. The best time resolution with the new bunching method is about 2.1 ns (FWHM) for an initial pulse duration of 300 ns. It is also seen that the shape and width of the distributions are affected by the cut, i.e., by the degree of monochromaticity of the moderated positrons, as expected from Liouville's theorem.

6.3. Experimental Results

6.3.1. Moderated positrons. It is well-known that the spectrum of the longitudinal energy of moderated positrons strongly depends on the quality of the moderator and can be significantly improved by annealing the W-film in situ (see, e.g., [130]). The moderator annealing in our setup was performed at 2000°C by bombarding the foil with an electron beam (≃25 W, 10 kV) for about 10 min in a vacuum of $\approx 10^{-8}$ mbar.

Figure 13a shows the dc positron intensity as a function of the potential difference ΔU between the moderator and the chopper grid. The maximum positron yield corresponds to moderator efficiency ~5.3×10^{-5}. The longitudinal energy spectra are obtained from the derivatives of the corresponding intensity curves and are shown in Fig. 13b. The spectra are taken before, ~1 h after and two days after the annealing. It is seen that the positron yield increases due to annealing almost by a factor two. The FWHM of the energy distributions also changes from ≃3 eV obtained before to ≃2 eV measured after annealing. The spectra taken two days after annealing illustrate degradation of the moderator surface through interactions with a residual gas, which results in a broadening of the energy spectrum and a more isotropic re-emission of the positrons, i.e., in an increase of the beam emittance.

6.3.2. Positron bunch width. In Fig. 14, the measured time distributions of pulsed positrons at the target are shown for an initial pulse of 90 ns and for different values of the retarding voltage between the moderator and the chopper grid. It is seen that the FWHM of the distributions is very sensitive to the energy spread ΔE of the moderated positrons changing from 1.4 to 0.63 ns for $\Delta E \sim 5$ V ($\Delta U = +1$ V) and $\Delta E \sim 1.5$ V ($\Delta U = -2.5$ V), respectively. It should be noted that the measurements shown in Fig. 13 were performed by the retarding potential method, using the grid as an energy analyzer. However, due to the inhomogeneity of the electric field formed by the grid, this method probably does not have an energy resolution better than ~1 eV and a significant contribution to the FWHM of the positron energy spectra can be expected.

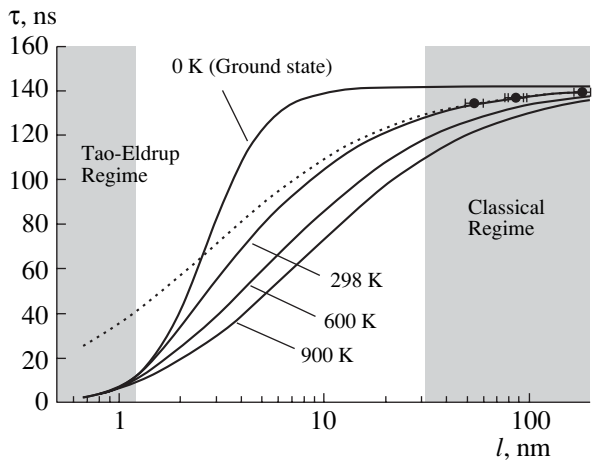

Fig. 17. Pore size as a function of *o*-Ps lifetime determined with the beam–PALS technique at different sample temperatures (see [144] for more details).

The measurement results demonstrate that the degree to which the positrons emitted from the moderator are monoenergetic is an important parameter. Thus, it is crucial to have a well-conditioned stable moderator in order to get a high performance of the beam. This observation is in qualitative agreement with the results of simulations.[10]

In Figs. 15a and 15b, the measured time distributions of positrons arriving at the MCP are shown for initial positron pulse durations of 300 and 120 ns, respectively. The FWHM of the distributions are estimated to be 2.3 and 1.4 ns. These values are comparable with those expected from Monte Carlo simulations (see, e.g., Fig. 12d). The compression ratio is ≃100, which is a factor of 5 better than the values previously obtained by Iijima et al. [124], reporting a compression from 50 to 2.2 ns, and by Tashiro et al. [134], reporting a compression from 30 to 1.4 ns, respectively. For the bunch width of ~2.3 ns and a repetition period of 1 μs, our pulsing efficiency is ≃31%, which is also a factor 6 better than reported in [124].

It should be noted that the peak to (flat) background ratio ($\simeq 10^2$) of the distributions shown in Figs. 15a and 15b is in agreement with expectations from the accidental coincidences of the START and STOP signals from (i) two different positrons, mostly due to the MCP detection inefficiency, or (ii) from nonpositron-related events due to the MCP noise. However, the non-Gaussian tails of the distributions in Figs. 15a and 15b (see also Fig. 18) are slightly worse than expected from simulations. There are several contributions to these tails due to: (i) the angular distribution of the moderated positrons and the fact that they are not monoenergetic; (ii) the extraction of slow positrons from the moderator; (iii) deviations of the pulse applied to the bunching electrodes from the calculated ideal shape; (iv) heterogeneous electric and magnetic fields; (v) time jitter of the detecting electronics, etc.

[10]The detail comparison of beam simulations and measurement results will be reported elsewhere.

7. MATERIAL SCIENCE WITH POSITRONS

The future of fundamental science is no longer determined by scientific challenges only. Today's society pushes science to strengthen the applications of its scientific achievements. Positron physics with monoenergetic beams of positrons is an excellent example illustrating developments in response to such demand.

Initially developed for fundamental atomic physics experiments, the slow positron beam technique has undergone very rapid development during the past several years toward numerous increasingly important applications. Due to the fact that positrons are the most sensitive probe of the electron density in materials, this technique became a unique tool for studying problems in basic and applied research in condensed matter physics and chemistry. Recently, its evolution to a phase of commercial exploitation has become notable.

Nowadays, there is a fundamental interest in studies of polymer surfaces [135], interfaces, and, in particular, of nanoporous materials which have attracted tremendous interest due to their many potential applications, including but not limited to low-dielectric constant (low-*k*) thin films in the microelectronic industry, membranes, and selective permeation filters in biotechnology, and catalysts in chemical engineering [136–141].

Porous SiO_2 films have been recently developed as low-dielectric interlayer insulators for use in future high-speed microelectronic devices. Voids are fabricated in these films in order to obtain a high degree of porosity and, hence, to make the dielectric constant lower. Important pore characteristics of the films, such as average size and size distributions, which have clear relation with the dielectric constant, are difficult to measure with standard techniques [142]. The emerging field of engineered nanoporosity (controlling pores from several angstroms to tens of nanometers) requires vast improvements in pore characterization techniques, as there are few probes capable of characterizing such porosity, especially in thin films and especially when the pores are closed and inaccessible to gas absorption techniques.

The positron annihilation lifetime spectroscopy (PALS) is a well-known and increasingly important (though less standard) technique that can be efficiently used to characterize the free-volume structure of such thin films (see, e.g., [136]). This technique uses either positrons emitted from a radioactive isotope (so-called classic PALS) or positrons delivered by an intense pulsed positron beam with energy variables typically in the range 1–50 keV [141].

In classic PALS setups, the timing start signal t_0 is provided by a γ-ray that is released coincidentally from a radioactive source (typically ^{22}Na) with the positron.

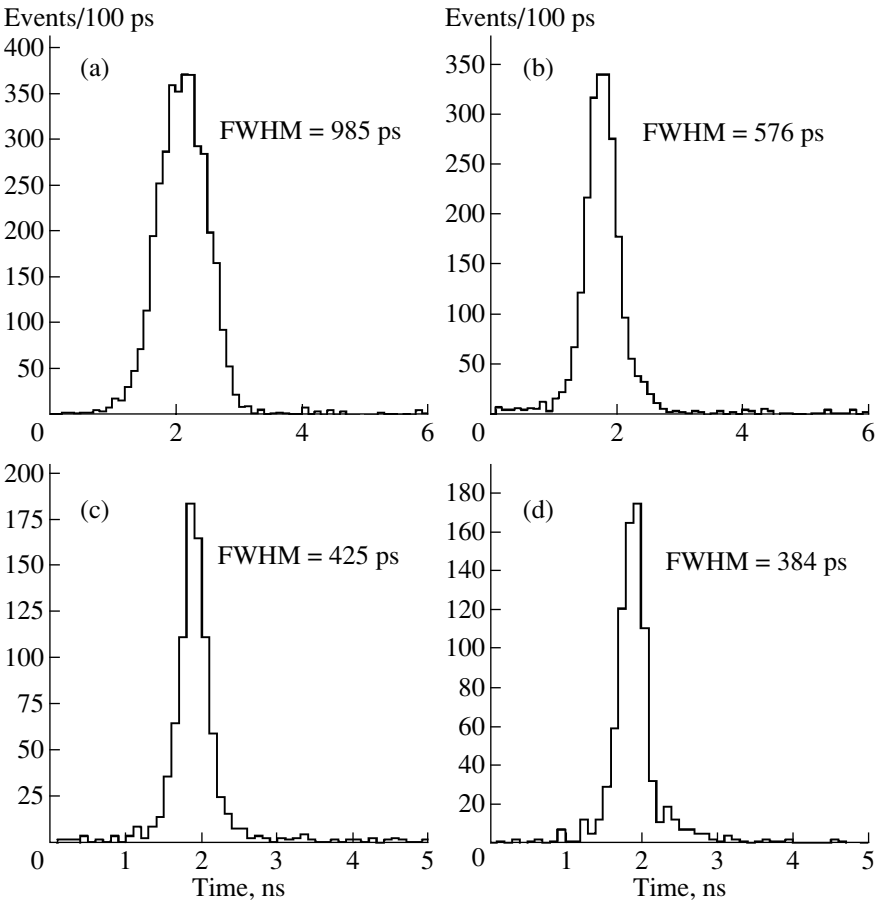

Fig. 18. Time distribution of bunched positrons at the target for a bunch pulse width corresponding to an initial positron pulse of 90 ns and chopper pulse durations of (a) 80, (b) 70, (c) 60, and (d) 50 ns, respectively. See text for details.

The stop signal is provided by one of the annihilation γ-rays. The *advantages* of this type of PALS technique are a high counting rate and a relatively simple experimental apparatus. The *disadvantage* is that the positrons are implanted relatively deeply and in an uncontrolled fashion, so that only the *average* properties of a sample can be studied with such a technique. Thus, this scheme is well suited for the investigation of the bulk materials, but not for the thin-film samples. In contrary, the *major advantage* of the PALS beam technique is the ability to control positron implantation into the sample. The sample can be depth-profiled by varying the incident beam energy [141].

The beam-based PALS technique has been recently reported as promising for testing pore sizes in the range from 0.3 to 100 nm for porous films with the thickness less than 0.1 μm [145, 146]. Details about the PALS technique and the methodologies of using beam PALS to explore nanoporous thin films are described in related publications [144, 148].

The spectra collected from PALS experiments are usually composed of a number of exponentially decaying functions, attributed to the annihilation of positrons from different states in a sample. Positron and positronium annihilation are represented in lifetime spectra by at least three exponentials that characterize the annihilation rate of positrons and para- and orthopositronium in a material sample.

Orthopositronium, as a most long-lived state, is formed and diffuses to low electron density sites, i.e., cavities or holes, in thin films. The annihilation of orthopositronium implies a pickoff process of an electron in the void or pore walls by the positron involved. The vacuum value of the *o*-Ps lifetime is shortened by this collisional pickoff annihilation and ranges typically from a fraction of a ns to tens of ns (see, e.g., [141]).

What is important is that the lifetime τ_3 of *o*-Ps in a sample is directly correlated to the radius of free-volume holes R_f. For example, in the so-called Tao–Eldrup regime [144], τ_3 (in ns) is related to R_f (in Å) through the following equation [136]:

$$\tau_3 = 0.5\left[1 - \frac{R_f}{R_f + 1.66} + \frac{1}{2\pi}\sin\left(2\pi\frac{R_f}{R_f + 1.66}\right)\right]^{-1}. \quad (71)$$

Therefore, this relation provides the *key* physical information concerning free volumes in thin films. As one can see from Eq. (71), in order to be sensitive to the

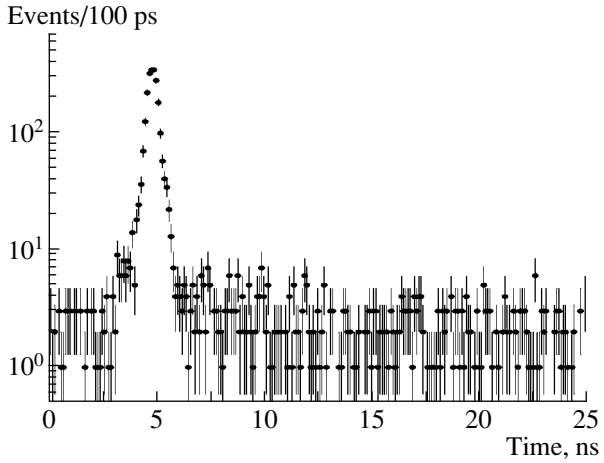

Fig. 19. Time distribution of positrons at the target with a FWHM of 576 ps.

pore size of ≃0.1–1 nm, the corresponding exponential with the lifetime of the order of $\tau_3 \simeq$ a few ns has to be resolved in a PALS lifetime spectrum.

An example of a porous SiO_2 film[11] is shown in Fig. 16. One may compare the resolution of pore sizes obtained with the SEM (scanning electron microscope) with the one accessible to the beam-PALS technique as illustrated in Fig. 17 [144].

The positron annihilation technique based on the use of monoenergetic slow positron beams is now established as one of the best methods for the investigation and control of defects in materials because of its very high level of sensitivity. For example, its high sensitivity to control defect concentrations from 10^{-8} to 10^{-3} by using a variable energy monoenergetic positron beam makes it a unique diagnostic and research tool with great promise, ideally suited for studying thin films, multilayer structures, and interfaces used in modern industry.

7.1. Possible Applications of the Developed Pulsed Beam

For high-quality PALS spectra measurements, the important characteristics of the positron bunch at the sample are: (i) the bunch width, typically <1 ns; (ii) peak to background ratio, typically $\geq 10^2$ (this is an important factor for accurate measurements of low-intensity *o*-Ps components); and (iii) shape of the time profile (resolution function), typically one or two Gaussians with small tails. The latter is important for measurements of short *o*-Ps lifetimes.

The flexibility of the developed pulsing scheme encourages us to test the generation of positron pulses with width <1 ns. To avoid the influence of significant bunching pulse distortions on the positron time profile at the target, we try to eliminate them by using only a part of the bunching pulse, where the aberrations of the shape are within a few percent (typically, the aberrations were significant at the beginning and at the end of the pulse). For this purpose, the initial positron pulse was shortened to a desired duration by the chopper pulse in such a way that the chopped positrons passing the bunching electrode received the correct bunching voltage from the selected (central) part of the buncher pulse, where aberration effects are negligible.

In Fig. 18, the results of these tests are shown for different chopper pulse durations, varying from 80 to 50 ns, and a bunch pulse width corresponding to an initial positron pulse of 90 ns. It is seen that a positron bunch width as short as ≃400 ps can be obtained with this pulsing method. In Fig. 19, the time distribution in Fig. 18b is shown with a logarithmic scale for more details. Although it has low statistics (because of the small ^{22}Na source activity, the counting rate is just ~1 Hz), the FWHM and the peak-to-background ratio (~10^2) are compatible with the ones typically obtained with the pulsed beam for application to polymer films (see, e.g., [134][12]).

We think that further increasing the statistics with a higher activity source, e.g., using the radioisotope ^{18}F [149], and an improvement of the time profile of the bunched positrons will result in a suitable beam for applications on thin film measurements.

8. CONCLUSIONS

Due to its specific properties, orthopositronium is an important probe of QED and also physics beyond the Standard Model. In this paper, we have reviewed phenomenological models of rare *o*-Ps decay modes. There are several interesting models, in particular, the mirror matter model and models with additional dimensions that predict the effect of the orthopositronium disappearance. The experimental signature of this effect is the invisible decay of orthopositronium, which may well occur at a rate within several (two or three) orders of magnitude of the present experimental upper limit.

We believe that this demonstrates the need for more sensitive methods of searching for *o*-Ps $\longrightarrow$ *invisible* decay to be developed in future experiments. It also suggests additional directions in searching for new physics in nonaccelerator experiments. Given the indications for the mirror world coming from dark matter and neutrino physics, as well as the intuitive expectation that nature could be left–right symmetric, it is obviously important to determine experimentally

[11]The sample was grown in the Institute of Microelectronic Technology (Moscow) [143].

[12]We assume that the convolution of this spectrum with a time resolution of ≃200–300 ps of a fast BaF_2 γ-detector, usually used for PALS measurements, will not significantly affect the FWHM of the spectrum.

whether orthopositronium is a window on the mirror world.

The corresponding experiments require the development of a high-efficiency pulsed slow positron beam, which could also be used for numerous important industrial applications as a unique diagnostic and research tool.

We have described the recently constructed high-efficiency pulsed slow positron beam for experiments with orthopositronium in vacuum. The new pulsing scheme is based on a double-gap coaxial buncher powered by an RF pulse of a specially designed shape, which is produced by an arbitrary waveform generator. With the modulation of the positron velocity in two gaps, their time of flight to a target is adjusted. This pulsing scheme makes it possible to minimize nonlinear aberrations in the bunching process and to achieve a compression ratio limited mainly by the intrinsic energy spread of the initial positrons. The flexibility of the new scheme makes it possible to efficiently compress the positron pulse with an initial pulse duration ranging from ~300 to 50 ns into a bunch of 2.3 to 0.4 ns in width. A compression ratio of $\simeq$100 and a pulsing efficiency of $\simeq$30% were achieved for a repetition period of 1 μs, which is five to six times better than previously reported numbers.

Both simulation and measurement results demonstrate that (i) the degree to which the positrons emitted from the moderator are monoenergetic and (ii) the precision of the bunching pulse waveform are important for the high performance of the beam. This will require the possible construction of a new, well-conditioned moderator with narrow ($\leq$1 eV) longitudinal energy spread of moderated positrons. In general, the developed beam is suitable for experiments with *o*-Ps in vacuum, mentioned above.

Preliminary results on the generation of short positron bunches for PALS applications to materials science are encouraging. However, further work to increase the beam intensity and possibly to improve the time profile of bunched positrons is required.

ACKNOWLEDGMENTS

We would like to thank N. Alberola, A. Badertsher, C. Bath, A.S. Belov, Z. Berezhiani, P. Crivelli, M. Felcini, R. Foot, U. Gendotti, N.A. Golubev, S.G. Karshenboim, M.M. Kirsanov, V.A. Kuzmin, V.A. Rubakov, V.V. Samoylenko, D. Sillou, and P. Tinyakov for valuable discussions and collaborations. We are grateful to I.N. Meshkov for thoughtful reading of the manuscript and useful remarks. The crucial assistance of A.S. Belov, N.A. Golubev, M.M. Kirsanov, L.L. Kurchaninov, and L. Knecht in the design and construction of the beam and electronics is gratefully acknowledged. The work of N.V. Krasnikov and V.A. Matveev was supported by the Russian Foundation for Basic Research (project nos. 03-02-16933 and 04-02-16020).

REFERENCES

1. M. Deutsch, Phys. Rev. **82**, 455 (1951).
2. *Proceedings of the Workshop on Positronium Physics, ETH Zürich, Switzerland, 2003* Ed. by M. Felcini, S. N. Gninenko, A. Nyffeler, and A. Rubbia, Int. J. Mod. Phys. A **19**, 3769 (2004).
3. I. N. Meshkov, Phys. Part. Nucl. **28**, 198 (1997).
4. S. G. Karshenboim, hep-ph/0509010.
5. M. I. Dobroliubov, S. N. Gninenko, A. Yu. Ignatiev, and V. A. Matveev, Int. J. Mod. Phys. A **8**, 2859 (1993).
6. A. Rich, Rev. Mod. Phys. **53**, 127 (1981).
7. V. V. Dvoeglazov, R. N. Faustov, and Y. N. Tyukhtyaev, Mod. Phys. Lett. A **8**, 3263 (1993).
8. S. N. Gninenko, N. V. Krasnikov, and A. Rubbia, Mod. Phys. Lett. A **17**, 1713 (2002).
9. A. Rubbia, Int. J. Mod. Phys. A **19**, 3961 (2004); in *Proceedings of the Workshop on Positronium Physics, ETH Zürich, Switzerland, 2003*; hep-ph/0402151.
10. S. G. Karshenboim, Int. J. Mod. Phys. **A19**, 3879 (2004); in *Proceedings of the Workshop on Positronium Physics, ETH Zürich, Switzerland, 2003*; hep-ph/0310099.
11. M. Skalsey, Mater. Sci. Forum **255-257**, 209 (1997).
12. P. A. Vetter, Mod. Phys. Lett. A **19**, 871 (2004); Int. J. Mod. Phys. A **19**, 3865 (2004).
13. A. A. Penin, hep-ph/0308204.
14. W. E. Caswell, G. P. Lepage, and J. Sapirstein, Phys. Rev. Lett. **38**, 488 (1977); G. S. Adkins, Phys. Rev. Lett. **76**, 4903 (1996).
15. I. Harris and L. M. Brown, Phys. Rev. **105**, 1656 (1957).
16. W. E. Caswell and G. P. Lepage, Phys. Rev. A **20**, 36 (1979).
17. I. B. Khriplovich and A. S. Yelkhovsky, Phys. Lett. B **246**, 520 (1990).
18. G. S. Adkins, R. N. Fell, and J. Sapirstein, Phys. Rev. Lett. **84**, 5086 (2000); Phys. Rev. A **63**, 032511 (2001).
19. A. Czarnecki, K. Melnikov, and A. Yelkhovsky, Phys. Rev. Lett. **83**, 1135 (1999); Phys. Rev. A **61**, 052502 (2000); G. S. Adkins, N. M. McGovern, R. N. Fell, and J. Sapirstein, hep-ph/0305251.
20. S. G. Karshenboim, Sov. Phys. JETP **76**, 541 (1993); Zh. Eksp. Teor. Fiz. **103**, 1105 (1993).
21. B. A. Kniehl and A. A. Penin, Phys. Rev. Lett. **85**, 1210 (2000); **85,** 3065(E) (2000); R. Hill and G. P. Lepage, Phys. Rev. D **62**, 111301 (2000); K. Melnikov and A. Yelkhovsky, Phys. Rev. D **62**, 116003 (2000).
22. G. S. Adkins and F. R. Brown, Phys. Rev. A **28**, 1164 (1983); G. P. Lepage, P. B. Mackenzie, K. H. Streng, and P. M. Zerwas, Phys. Rev. A **28**, 3090 (1983); G. S. Adkins and E. D. Pfahl, Phys. Rev. A **59**, R915 (1999).
23. G. S. Adkins, R. N. Fell, and J. Sapirstein, Ann. Phys. (N.Y.) **295**, 136 (2002).
24. S. Asai, S. Orito, and N. Shinohara, Phys. Lett. B **357**, 475 (1995); S. Asai, O. Jinnouchi, and T. Kobayashi, hep-ex/0308030.
25. R. S. Vallery, P. W. Zitzewitz, and D. W. Gidley, Phys. Rev. Lett. **90**, 203402 (2003).
26. A. H. Al-Ramadhan and D. W. Gidley, Phys. Rev. Lett. **72**, 1632 (1994).

27. D. Sillou, Int. J. Mod. Phys. A **19**, 3919 (2004); in *Proceedings of the Workshop on Positronium Physics, ETH Zürich, Switzerland, 2003*.
28. C. I. Westbrook, D. W. Gidley, R. S. Conti, and A. Rich, Phys. Rev. Lett. **58**, 1328 (1987).
29. C. I. Westbrook, D. W. Gidley, R. S. Conti, and A. Rich, Phys. Rev. A **40**, 5489 (1989).
30. J. S. Nico, D. W. Gidley, A. Rich, and P. W. Zitzewitz, Phys. Rev. Lett. **65**, 1344 (1990).
31. O. Jinnouchi, S. Asai, and T. Kobayashi, hep-ex/0011011.
32. O. Jinnouchi, S. Asai, and T. Kobayashi, Int. J. Mod. Phys. A **19**, 3927 (2004); in *Proceedings of the Workshop on Positronium Physics, ETH Zürich, Switzerland, 2003*; Phys. Lett. B **572**, 117 (2003).
33. A. P. Mills, Jr. and G. H. Bearman, Phys. Rev. Lett. **34**, 246 (1975); A. P. Mills, Jr., Phys. Rev. A **27**, 262 (1983).
34. M. W. Ritter, P. O. Egan, V. W. Hughes, and K. A. Woodle, Phys. Rev. A **30**, 1331 (1984).
35. R. Karplus and A. Klein, Phys. Rev. **87**, 848 (1952).
36. G. T. Bodwin and D. R. Yennie, Phys. Rep. **43**, 267 (1978).
37. S. J. Brodsky and G. W. Erickson, Phys. Rev. **148**, 26 (1966); R. Barbieri, J. A. Mignaco, and E. Remiddi, Nuovo Cimento A **11**, 824 (1972).
38. G. S. Adkins, M. H. T. Bui, and D. Zhu, Phys. Rev. A **37**, 4071 (1988); G. S. Adkins, Y. M. Aksu, and M. H. T. Bui, Phys. Rev. A **47**, 2640 (1993); G. S. Adkins, R. N. Fell, and P. M. Mitrikov, Phys. Rev. Lett. **79**, 3383 (1997); A. H. Hoang, P. Labelle, and S. M. Zebarjad, Phys. Rev. Lett. **79**, 3387 (1997).
39. J. R. Sapirstein, E. A. Terray, and D. R. Yennie, Phys. Rev. D **29**, 2290 (1984); K. Pachucki and S. G. Karshenboim, Phys. Rev. Lett. **80**, 2101 (1998).
40. K. Pachucki, Phys. Rev. A **56**, 297 (1997); G. S. Adkins and J. Sapirstein, Phys. Rev. A **58**, 3552 (1998); **61**, 069902(E) (2000); A. P. Burichenko, Yad. Fiz. 64, 1709 (2001) [Phys. Atom. Nucl. **64**, 1628 (2001)].
41. A. Czarnecki, K. Melnikov, and A. Yelkhovsky, Phys. Rev. Lett. **82**, 311 (1999); Phys. Rev. A **59**, 4316 (1999).
42. R. J. Hill, Phys. Rev. Lett. **86**, 3280 (2001); K. Melnikov and A. Yelkhovsky, Phys. Rev. Lett. **86**, 1498 (2001); B. A. Kniehl and A. A. Penin, Phys. Rev. Lett. **85**, 5094 (2000).
43. T. Kinoshita and M. Nio, Phys. Rev. Lett. **72**, 3803 (1994); M. I. Eides and V. A. Shelyuto, Pis'ma Zh. Eksp. Teor. Fiz. **61**, 465 (1995) [JETP Lett. **61**, 478 (1995)]; Phys. Rev. A **52**, 954 (1995); K. Pachucki, Phys. Rev. A **54**, 1994 (1996).
44. M. Nio and T. Kinoshita, Phys. Rev. D **55**, 7267 (1997).
45. A. Billoire, R. Lacaze, A. Morel and H. Navelet, Phys. Lett. B **78**, 140 (1978); T. Muta and T. Niuya, Prog. Theor. Phys. **68**, 1735 (1982); G. S. Adkins and F. R. Brown, Phys. Rev. A **28**, 1164 (1983); G. P. Lepage et al., Phys. Rev. A **28**, 3090 (1983); S. Adachi, BSc Thesis (Metropolitan University, Tokyo, 1990).
46. G. S. Adkins and E. D. Pfahl, Phys. Rev. A **59**, R915 (1998).
47. G. P. Lepage et al., Phys. Rev. A **28**, 3090 (1983); G. S. Adkins and F. R. Brown, Phys. Rev. A **28**, 1164 (1983).
48. T. Matsumoto et al, Phys. Rev. A **54**, 1947 (1996).
49. A. Czarnecki and S. G. Karshenboim, hep-ph/9911410.
50. U. Amaldi, G. Carboni, B. Jonson, and J. Thun, Phys. Lett. B **153**, 444 (1985).
51. J. Yang et al., Phys. Rev. A **54**, 1952 (1996).
52. D. W. Gidley, J. S. Nico, and M. Scalsey, Phys. Rev. Lett. **66**, 1302 (1991).
53. S. Asai et al., Phys. Rev. Lett. **66**, 1298 (1991).
54. S. Asai et al., Phys. Rev. Lett. **66**, 2240 (1991).
55. S. Asai et al., Phys. Lett. B **323**, 90 (1994).
56. M. Tsuchiaki et al., Phys. Lett. B **236**, 81 (1990).
57. M. V. Akopyan et al., Phys. Lett. B **272**, 443 (1991).
58. T. Maeno et al., Phys. Lett. B **351**, 574 (1995).
59. S. N. Gninenko, Yu. M. Klubakov, A. A. Poblaguev, and V. E. Postoev, Phys. Lett. B **237**, 287 (1990).
60. T. Mitsui et al., Europhys. Lett. **33**, 111 (1996).
61. M. Skalsey and R. S. Conti, Phys. Rev. D **51**, 6292 (1995).
62. R. Escribano, E. Masso, and R. Toldra, Phys. Lett. B **356**, 313 (1995).
63. T. Mitsui et al., Phys. Rev. Lett. **70**, 2265 (1993).
64. A. Badertscher et al., Phys. Lett. B **452**, 29 (2002); P. Crivelli, Can. J. Phys. **80**, 1281 (2002).
65. G. S. Atojan, S. N. Gninenko, V. I. Razin, and Yu. V. Ryabov, Phys. Lett. B **220**, 317 (1989).
66. P. A. Vetter and S. J. Freedman, Phys. Rev. A **66**, 052505 (2002).
67. N. V. Krasnikov, Int. J. Mod. Phys. A **19**, 3849 (2004); in *Proceedings of the Workshop on Positronium Physics, ETH Zürich, Switzerland, 2003*.
68. P. A. Vetter, Mod. Phys. Lett. A **19**, 871 (2004).
69. W. Bernreuther and O. Nachttmann, Z. Phys. C **11**, 235 (1981).
70. B. K. Arbic et al., Phys. Rev. A **37**, 3189 (1988).
71. M. Scalsey and J. Van House, Phys. Rev. Lett. **67**, 1993 (1991).
72. M. Felcini, Int. J. Mod. Phys. A **19**, 3853 (2004); in *Proceedings of the Workshop on Positronium Physics, ETH Zürich, Switzerland, 2003*; hep-ex/0404041.
73. B. Holdom, Phys. Lett. B **166**, 196 (1986).
74. S. Davidson, S. Hannestad, and G. Raffelt, J. High Energy Phys. **0005**, 003 (2000); hep-ph/0001179.
75. M. I. Dobroliubov and A. Yu. Ignatiev, Phys. Rev. Lett. **65**, 679 (1990).
76. A. A. Prinz et al., Phys. Rev. Lett. **81**, 1175 (1998).
77. T. D. Lee and C. N. Yang, Phys. Rev. **104**, 254 (1956).
78. L. B. Okun, Int. J. Mod. Phys. A **17** (Suppl. 1), 105 (2002); hep-ph/0112031.
79. I. Kobzarev, L. Okun, and I. Pomeranchuk, Sov. J. Nucl. Phys. **3**, 837 (1966).
80. R. Foot, H. Lew, and R. R. Volkas, Phys. Lett. B **272**, 67 (1991).
81. Z. Berezhiani and R. Mohapatra, Phys. Rev. D **62**, 6607 (1995); E. Akhmedov, Z. Berezhiani, and G. Senjanovic, Phys. Rev. Lett. **69**, 3013 (1992); Z. Berezhiani, A. Dolgov, and R. N. Mohapatra, Phys. Lett. B **375**, 26 (1996); Z. Berezhiani, Acta Phys. Pol. B **27**, 1503 (1996).

82. Z. Berezhiani, Int. J. Mod. Phys. A **19**, 3775 (2004); in *Proceedings of the Workshop on Positronium Physics, ETH Zürich, Switzerland, 2003*; hep-ph/0312335.
83. R. Foot, Int. J. Mod. Phys. A19, 3807 (2004); in *Proceedings of the Workshop on Positronium Physics, ETH Zürich, Switzerland, 2003*; astro-ph/0309330.
84. Z. Berezhiani, hep-ph/0508233; Z. Berezhiani, P. Ciarcelluti, D. Comelli, and F. L. Villante, Int. J. Mod. Phys. D **14**, 107 (2005); astro-ph/03126053; P. Ciarcelluti, astro-ph/040963, astro-ph/0409630, astro-ph/0409629, astro-ph/0312607; R. Foot, astro-ph/0407623, astro-ph/0403043, astro-ph/0406257; R . Foot and R. R. Volkas, Phys. Rev. D **69**, 123510 (2004); astro-ph/0407522; R. Foot and Z. K. Silagadze, astro-ph/0404515; S. L. Dubovsky and S. M. Sibiryakov, Nucl. Phys. B **691**, 91 (2004); L. Bento and Z. Berezhiani, Phys. Rev. Lett. **87**, 231304 (2001); hep-ph/0107281; A. Yu. Ignatiev and R. R. Volkas, Phys. Rev. D **68**, 023518 (2003), hep-ph/0304260.
85. R. Barbieri, T. Gregoire, and L. J. Hall, Preprint CERN-PH-TH-2005-162 (2005); hep-ph/0509242; Z. Chacko, Hock-Seng Goh, and R. Harnik, hep-ph/0506256; Z. Berezhiani and L. Bento, hep-ph/0507031; A. Yu. Ignatiev and R. R. Volkas, Phys. Lett B **487**, 294 (2000); hep-ph/0005238.
86. R. Foot, Acta Phys. Pol. B **32**, 2253 (1991).
87. R. Foot and S. N. Gninenko, Phys. Lett. B **480**, 171 (2000).
88. R. Foot, A. Yu. Ignatiev, and R. R. Volkas, Phys. Lett. B **503**, 355 (2001) astro-ph/0011156.
89. S. L. Glashow, Phys. Lett. B **167**, 35 (1986).
90. S. N. Gninenko, Phys. Lett. B **326**, 317 (1994).
91. R. Foot, Phys. Rev. D **69**, 036001 (2004); hep-ph/0308254.
92. R. Bernabei et al. (DAMA Collab.), Riv. Nuovo Cimento **26**, 1 (2003); astro-ph/0307403, and references therein.
93. E. D. Carlson and S. L. Glashow, Phys. Lett. B **193**, 168 (1987).
94. E. W. Kolb, R. N. Mohapatra, and V. L. Tepliz, Phys. Rev. Lett. **77**, 3066 (1996).
95. Z. Berezhiani, D. Comelli, and F. L. Villante, Phys. Lett. B **503**, 362 (2001).
96. S. N. Gninenko and N. V. Krasnikov, Phys. Lett. B **513**, 119 (2001).
97. S. Davidson et al., J. High Energy Phys. **0202**, 037 (2002).
98. E. D. Carlson, Nucl. Phys. B **286**, 378 (1987); M. I. Dobroliubov and A. Yu. Ignatiev, Nucl. Phys. B **309**, 655 (1988); M. I. Dobroliubov, Yad. Fiz. **52**, 551 (1990) [Sov. J. Nucl. Phys. **52**, 352 (1990)]; S. N. Gninenko and N. V. Krasnikov, Phys. Lett. B **427**, 307 (1988); S. N. Gninenko and N. V. Krasnikov, Phys. Lett. B **434**, 163 (1998).
99. L. Randall and R. Sundrum, Phys. Rev. Lett. **83**, 3370 (1990); Phys. Rev. Lett. **83**, 4690 (1990);
100. V. A. Rubakov, Phys. Usp. **171**, 913 (2001); hep-ph/0105152.
101. I. Antoniadis, Phys. Lett. B **346**, 377 (1990).
102. N. V. Krasnikov, Phys. Lett. B **273**, 246 (1991).
103. N. Arkani-Hamed, S. Dimopoulos, and G. Dvali, Phys. Lett. B **429**, 263 (1998); I. Antoniadis et al., Phys. Lett. B **436**, 257 (1998); G. F. Guidice, R. Rattazzi and J. D. Wells, Nucl. Phys. B **544**, 3 (1999); G. F. Guidice, R. Rattazzi and J. D. Wells, Nucl. Phys. B **595**, 250 (2001).
104. S. L. Dubovsky, V. A. Rubakov, and P. G. Tinyakov, Phys. Rev. D **62**, 105011 (2000); hep-th/0006046.
105. S. N. Gninenko, N. V. Krasnikov, and A. Rubbia, Phys. Rev. D **67**, 075012 (2003).
106. L. B. Okun, hep-ph/0210052.
107. P. Crivelli, Int. J. Mod. Phys. A **19**, 3819 (2004); A. Badertscher et al., hep-ex/0404037.
108. A. Badertscher et al., hep-ex/0311031; S. N. Gninenko, Int. J. Mod. Phys. A **19**, 3833 (2004); in *Proceedings of the Workshop on Positronium Physics, ETH Zürich, Switzerland, 2003*.
109. S. N. Gninenko, Int. J. Mod. Phys. A **19**, 3939 (2004); in *Proceedings of the Workshop on Positronium Physics, ETH Zürich, Switzerland, 2003*.
110. A. Badertscher et al., "Development of a High-efficiency Pulsed Slow Positron Beam," submitted to Nucl. Instr. and Meth.
111. D. W. Gidley et al., Phys. Rev. B **60**, R5157 (1999).
112. http://lepta.jinr.ru.
113. I. N. Meshkov and A. N. Skrinsky, Nucl. Instrum. Methods Phys. Res. A **379**, 41 (1996).
114. I. N. Meshkov, Nucl. Instrum. Methods Phys. Res. B **221**, 168 (2004).
115. I. N. Meshkov, Nucl. Phys. **59**, 1523 (1996).
116. I. N. Meshkov, "Generation of Directed Flux of Positronium and Experimental Studies with Positronium in-flight", in *Proceedings of Workshop "Hadronic Atoms and Positronium in Standard Model", Dubna 1998*, p. 176.
117. S. B. Fedorenko et al., in *Proceedings of EPAC, Vienna, Austria, 2000*, p. 584.
118. I. N. Meshkov et al., Nucl. Instrum. Methods Phys. Res. B **214**, 186 (2004).
119. A. Badertscher et al., Int. J. Mod. Phys. A **19**, 3833 (2004); hep-ex/0311031.; S. N. Gninenko, Int. J. Mod. Phys. A **19**, 3939 (2004).
120. P. Willutzki et al., Meas. Sci. Technol. **5**, 548 (1994), and references therein.
121. R. Suzuki, T. Ohdaira, and T. Mikado, Radiat. Phys. Chem. **58**, 603 (2000), and references therein.
122. N. Oshima et al., Appl. Surf. Sci. **116**, 82 (1997).
123. E. Hamada et al., Radiat. Phys. Chem. **58**, 771 (2000).
124. H. Iijima et al., Nucl. Instrum. Methods Phys. Res. A **483**, 641 (2002).
125. N. Alberola et al., physics/0511048.
126. N. B. Chilton and P. G. Coleman, Meas. Sci. Technol. **6**, 53 (1995).
127. *Positron Beams and their Applications*, Ed. by P. Coleman (World Sci., Singapore, 2000).
128. M. Charlton and J. W. Humberston, *Positron Physics* (Cambridge Univ. Press, Cambridge, 2001).
129. M. Charlton, Nucl. Instrum. Methods B **143**, 11 (1998).
130. P. Schultz and K. G. Lynn, Rev. Mod. Phys. **60**, 701 (1988).

131. The simulation programm is based on GEANT 4, CERN Program Library Long Writeup W5013.

132. The code is courtesy of the group from the "Troitsk Neutrino Mass Experiment" at INR (Moscow).

133. www.amplifiers.com.

134. M. Tashiro et al., Radiat. Phys. Chem. **60**, 529 (2001).

135. C. Bas et al., "Positron Interaction in Polymers," Int. J. Mod. Phys. A **19**, 3951 (2004); in *Proceedings of the Workshop on Positronium Physics, ETH Zürich, Switzerland, 2003*.

136. Y. C. Jean, Mater. Sci. Forum **175-178**, 59 (1995); *Positron Spectroscopy of Solids,* Ed. by A. Dupasquier and A. P. Mills., Jr (IOS, Amsterdam), 503 (1995).

137. *Positron and Positronium Chemistry,* Ed. by H. J. Ache, D. M. Schrader, and Y. C. Jean (Elsevier, Holland, 1988), p. 318.

138. O. E. Mogensen, *Positron Annihilation in Chemistry* (Springer, Berlin, 1995), Springer Series in Chem. Phys., Vol. 58.

139. *Positron Beams and their Applications*, Ed. by P. Coleman (World Sci., Singapore, 2000).

140. V. I. Grafutin and E. P. Prokop'ev, Phys. Usp. **45**, 59 (2002).

141. *Principles and Applications of Positron and Positronium Chemistry*, Ed. by Y. C. Jean, P. E. Mallon, and D. M. Schrader (World Sci., Singapore, 2003).

142. D. W. Gidley et al., Phys. Rev. B **60**, R5157 (1999).

143. A. Mokrushin, I. Bardyshev, N. Serebryakova, and V. Starkov, Phys. Status Solidi A **197**, 212 (2003).

144. T. Dull et al., J. Phys. Chem. B **105**, 4657 (2001).

145. L. Xie at el., Phys. Rev. Lett. **74**, 4947 (1995).

146. G. B. DeMaggio et al., Phys. Rev. Lett. **78**, 1524 (1997).

147. J. N. Sun, Y. F. Hu, W. E. Frieze, and D. W. Gidley, Radiat. Phys. Chem. **68**, 345 (2003).

148. J. N. Sun, D. W. Gidley, Y. F. Hu, et al., Appl. Phys. Lett. **81**, 1447 (2002).

149. U. Gendotti, "18F Source for Positron Beams," PhD Thesis (ETH, Zürich, 2005).